1-1-1995

Angle beam synthetic aperture focusing in ultrasonics

Irfan M. Furniturewala
Iowa State University

Angle beam synthetic aperture focusing in ultrasonics

by

Irfan M. Furniturewala

A Thesis Submitted to the

Graduate Faculty in Partial Fulfillment of the

Requirements for the Degree of

MASTER OF SCIENCE

Department: Electrical and Computer Engineering
Major: Electrical Engineering

Approved:

Signatures have been redacted for privacy

Member of the Committee:

Signatures have been redacted for privacy

Iowa State University
Ames, Iowa
1995

TABLE OF CONTENTS

LIST OF FIGURES

ACKNOWLEDGEMENTS

First and foremost, I wish to thank God, for giving me all the wonderful opportunities, and the best family and colleagues.

I would like to take this space to extend my deep-felt gratitude towards my major professor, Dr. Lalita Udpa, for having the confidence and faith in me, and for providing me with valuable suggestions and critique, throughout my master's program. I also wish to offer my deepest thanks to my other committee members, Dr. Satish Udpa and Dr. Soma Chaudhuri, for their encouragement and help. I am thankful to the Electric Power Research Institute (EPRI), which was responsible for sponsoring this research. Especially, I wish to thank Mr. Tom Taylor at EPRI, for his complete guidance and support in all possible ways towards this research. I acknowledge the support of Mr. Mike Elmo at EPRI, for providing me with his PC_Image program, which served as a valuable tool during the entire research. I also thank Mr. Kevin Levesque at LMT, Inc. and Mr. Mark Davis at Davis NDE, Inc., for their time and suggestions on scanning techniques used in the industry. I express my deep gratitude, towards my colleagues, Dr. Mani Mina and Mr. Wassef Masri, who helped with the initial part of the research.

My parents, brothers and sister deserve a special acknowledgement for instilling in me the confidence, and providing me with the support, that I needed to pursue

this program. I am extremely thankful to them for being the most wondeful family. This space will not be complete without acknowledging the support of my dearest wife, Asma, who has played a very important role in all my achievemnets, and has made all the difference to my life. Last, but not the least, I thank my good friend, Ashish Dixit, for extending his support in ways more than one.

Thank you to all of the above people for their enthusiasm, and confidence in me.

CHAPTER 1. INTRODUCTION

Defects, big or small, can cause major disasters. Aircrafts have crashed, oil pipelines have ruptured and nuclear reactors have failed because of undetected cracks. In order to assess the safety of a part, it is important to establish (without damaging it) whether it contains structural defects, and if so, to decide whether it can continue to be used in operation. All this needs to be done without damaging the part. Non-destructive evaluation (NDE) techniques are used extensively to accomplish this inspection [1].

The aim of NDE is not to reject a product having a defect. This would imply that finding smaller flaws would lead to rejecting more parts. On the contrary, the aim of NDE is to characterize flaws and to evaluate their severity. Characterization of flaws implies determining their size, shape, orientation, etc. By characterizing the flaws, it is possible to quantify the safe limits for operation of the specimen being tested.

Many nondestructive (NDT) methods have reached the stage of development where they can be used by a semi-skilled operator following detailed procedural instructions, with safeguards built into the system. However, given the working conditions and the tedious nature of evaluation, the accuracy of operator interpretation can definitely be improved by enhancing the signals using signal and image processing

techniques. With rapid advances made in the field of Very Large Scale Integration (VLSI) technology, it is not inconceivable to have more sophisticated equipment to pre-process the large volume of data generated in real-time. This increases both the speed and the accuracy of evaluation of the operator, thus reducing inspection costs. During the last few years, the potential economic pay-off of NDE has been recognized. As a result there has been a tremendous emphasis on research towards improving all aspects of nondestructive testing. A variety of NDE techniques have been developed over the years to cater to a number of application problems. A brief summary of some of these methods is given below.

NDE Techniques

Generally, defects are characterized into three main groups. The groups are:

1. Inherent defects (resulting from the manufacture of the raw material).
2. Fabrication defects (resulting from the conversion of the raw material to a finished part).
3. Service induced defects (generated during the operation of a part) [2].

NDT techniques aim at detecting and characterizing all the above classes of defects. Some of the most commonly employed nondestructive techniques are ultrasonic, eddy current, magnetostatic, X-ray radiography and acoustic emission.

The ultrasonic testing method involves inducing high frequency (greater than 20 KHz) pulses into the specimen under test, and analyzing the reflected or scattered energy for defect characterization. Eddy current testing involves the interaction between an induced eddy current electromagnetic field and the test object. The

corresponding change in the impedance of the probe coil constitutes the eddy current signal, which contains information related to the condition of the specimen. In magnetostatic NDE, the specimen, which is ferromagnetic, is magnetized by suitable methods, and flaws at the surface or subsurface distort the magnetic field, causing local flux leakage fields. In X-ray radiography, X-rays are passed through the test specimen, and defects having a different density compared to the surrounding matter are revealed by a localized difference in the blackness of the film image. In acoustic emission NDE, the sound emitted by solids subjected to a high level of stress is analyzed for flaw characterization [3] [4].

Each of these NDT techniques have a wide range of applications and it is not easy to compare the overall performance of one NDT technique over others.

Problem Statement

The problem addressed in this thesis is one module of the overall system to automate flaw detection, location and classification in Boiling Water Reactors (BWR) tubings. Stainless steel pipes of thickness 0.69 inches, and an outer diameter of 12 inches are inspected for cracks using ultrasonic nondestructive testing methods. Cracks in these pipes, mainly develop close to the weld joining two pipes. Specifically, the cracks develop in the heat affected zone (HAZ) of the pipes. The heat affected zone extends axially upto 0.5 inches from the weld for thin pipes (thickness less than 0.5 inches) and upto 1.25 inches for thick pipes (thickness from 1.25 inches to 1.5 inches). A typical weld geometry is shown in Figure 1.1. The counterbore represents the thinning of the pipes to ensure that pipes being welded are of the same thickness.

Most of the cracks are due to mechanical fatigue, thermal fatigue, or intergranu-

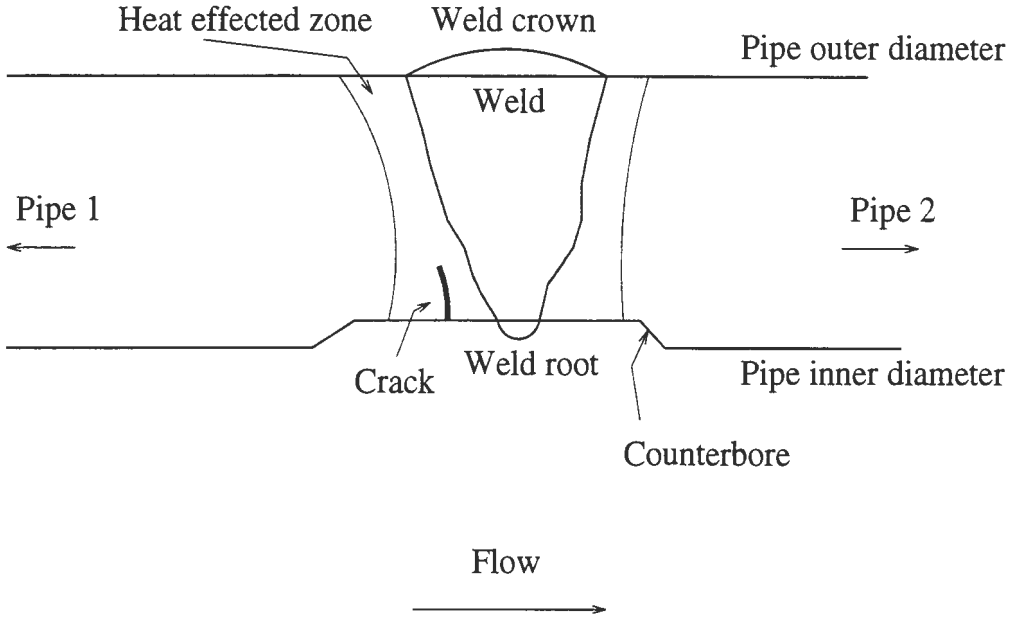

Figure 1.1: Typical nuclear pipe and weld geometry

lar stress corrosion. Each of these have a characteristic signature as far as the reflection and scattering of the induced signal is concerned. The pipes are tested for cracks using ultrasonic NDE techniques. A typical setup comprises of an operator in complete radiation-proof gear getting into the reactor, scanning the pipes in an attempt to characterize the reflected signal as being from counterbore, root-weld or crack. Due to the high noise environment of the setup, it is quite probable, even for a highly skilled operator, to misclassify the reflected signal. This may lead to catastrophic results. It is, therefore, necessary for some preprocessing to be performed before the operator interprets the signal. Synthetic aperture focusing technique (SAFT) is one such widely used method to enhance the signal to noise ratio (SNR) of ultrasonic and radar signals. Most of the research uptil now has concentrated on performing

SAFT on data collected using the normal mode of incidence of the ultrasonic beam. However, as will be discussed in later chapters, nuclear NDE uses the angle-beam mode of inspection of test specimens. There has not been much research done in this field. In this research, a SAFT algorithm has been developed for preprocessing the ultrasonic data collected using the angle-beam technique. The algorithm has been tested with ultrasonic signals from the industry, and initial results look promising, thus enhancing detectability of defects. Algorithms related to flaw location have also been developed in this research. These algorithms are valuable in locating and characterising the defects, and other features of the specimen being evaluated.

The thesis is organized as follows. Chapter 2 provides information on the various techniques and modes of ultrasonic NDE data collection and representation. A discussion on the principles and formulation of normal SAFT is given in chapter 3. Chapter 4 describes angle-beam SAFT in detail and presents the algorithm used in the research. A discussion of the results along with conclusions and areas for further investigation are presented in Chapter 5.

CHAPTER 2. ULTRASONIC NONDESTRUCTIVE EVALUATION

Ultrasound, as used in nondestructive testing, refers to sound waves slightly above the audible range of the human ear, i.e. greater than 20 KHz. For years, ultrasound has been used to cover all aspects of NDT research, ranging from the detection of internal crack in materials to small sub-surface defects. These methods have played a major role in the quality inspection of partially manufactured components, as well as nondestructive testing of parts being used.

There are several modes of ultrasound propagation. The generation and propagation of ultrasonic waves is considered in the next section [5].

Generation and Propagation of Ultrasonic Waves

Crystals of certain minerals and salts, when subjected to alternating electric charges, expand and contract under the influence of these charges. Conversely, these materials when subject to alternate compression and tension generate alternating charges. This is the piezo electric effect. A large number of piezo-electric materials, including man-made ceramics and polymers, have been used in the construction of modern ultrasound transducers. However, the original material used was, and still is, natural quartz. When a piezo electric material is subject to an alternating voltage across its thickness, vibrations, caused by contraction and expansion of the disc,

gives rise to a compressional wave normal to the disc's surface. When the transducer crystal vibrates at it's natural frequency, wave generation is most efficient. Piezo electric materials can be used for generating as well as detecting sound waves [5].

Ultrasonic waves are elastic waves, which can be transmitted through any medium. However, a required criteria for the propagation of ultrasonic waves is that the medium should be continuous for the energy to propagate freely. Any discontinuity, such as internal voids, delaminations or cracks, will interfere with the transmission of ultrasonic signals.

UT waves propagate in two dominant modes, namely longitudinal and shear. In fluid medium, ultrasonic waves propagate in the longitudinal or compressional mode, wherein the wave propagates in the direction of particle vibration [6]. However, in solids, a shear wave component may arise, wherein the wave displacement is normal to the direction of propagation. Elastic surface waves, called Rayleigh waves can also occur.

The longitudinal mode of wave transmission is probably the most widely used in ultrasonic testing. In most common materials, this wave has a short wave length in comparison with the cross sectional area of the transducer. Consequently, the wave energy is focused into a sharp beam with a small divergence. The main use of longitudinal waves is for the detection and location of cracks that present a reasonably large frontal area to the test surface. In fluids the longitudinal velocity ϑ_l of ultrasound waves is given by

$$\vartheta_l = \sqrt{\frac{\gamma_a}{\rho}} \tag{2.1}$$

where γ_a is the adiabatic volume elasticity, and ρ is the density of the fluid. However, for solids the expression for the longitudinal velocity is not as trivial. The longitudinal

velocity ϑ_l in the case of solids is given by

$$\vartheta_l = \sqrt{\frac{\epsilon(1-\kappa)}{\rho(1+\kappa)(1-2\kappa)}} \tag{2.2}$$

where ϵ is the Young's modulus of elasticity, κ is the Poisson's ratio and ρ is the density of the solid.

Shear waves have lower velocities than longitudinal waves. As a result, shear waves have shorter wavelengths than longitudinal waves of the same frequency. This shorter wavelength makes shear waves more sensitive to smaller defects, and consequently they are more easily scattered within the specimen. Shear beams are mainly used for inspection with the angle-beam technique. The shear wave velocity ϑ_s of propagation of ultrasound in solids is is given by

$$\vartheta_s = \sqrt{\frac{\zeta}{\rho}} \tag{2.3}$$

where ζ is the modulus of rigidity of the material.

As sound propagates through a material it is attenuated with the distance of propagation z [7], according to the equation

$$I = I_0 e^{-\alpha z} \tag{2.4}$$

where I is the intensity at depth z and I_0 is the intensity at the surface of the material ($z = 0$). The attenuation coefficient, α, depends on the frequency, and increases with an increase in the frequency. However, the frequency f, along with the velocity of sound, ϑ, in a specific medium, determine the wavelength, λ, of the ultrasonic pulse. Note that the wavelength must be kept as short as possible to improve axial

resolution [8]. These three variables are related by the following equation

$$\lambda = \frac{\vartheta}{f} \tag{2.5}$$

It can be verified that higher the frequency, lower the wavelength, the better the resolution. The trade-off is the high attenuation at higher frequencies.

Comparison of Ultrasonic NDT with other Techniques

Ultrasound inspection has several distinct advantages over other NDT methods [2]. Among the most significant are:

1. The inspection requires only one surface for inspection.
2. The ability of ultrasonic test waves to penetrate thick specimen.
3. Its ability to locate the exact position of a flaw.
4. The capability to detect minute flaws under appropriate conditions.
5. The compatibility of ultrasonic inspection for automated processing.

Ultrasonics, as do other NDT methods, has disadvantages, which require consideration. Among these are:

1. The test object must be able to conduct sound without excessive losses.
2. Discontinuities just beneath the surface (dead zone) may not be detectable.
3. Need for qualified technical personnel to operate and interpret the information resulting from an ultrasonic inspection.

4. The geometry of the test piece may make ultrasonic inspection difficult or impossible.

5. The necessity of a good contact for the sound to be transmitted into and returned from the test piece.

6. The relatively small area of inspection due to the small area of the search unit. This limitation makes the inspection of large surfaces dependent on using multiple transducers and complicated mechanical scanning equipment [2].

Ultrasonic Testing Techniques

There are two methods for carrying out a UT inspection:

1. Pulse-echo

2. Pitch-catch

Both these methods rely upon the fact that inhomogeneities produce variations in impedance of the surrounding media [4]. Each of these is detailed in the following subsections.

Pitch-catch technique

In the pitch-catch or through-transmission mode of UT testing, two transducers are applied on either side of the specimen under test as shown in Figure 2.1. This in turn requires both surfaces of the test piece to be accessible, which may not be possible in some cases.

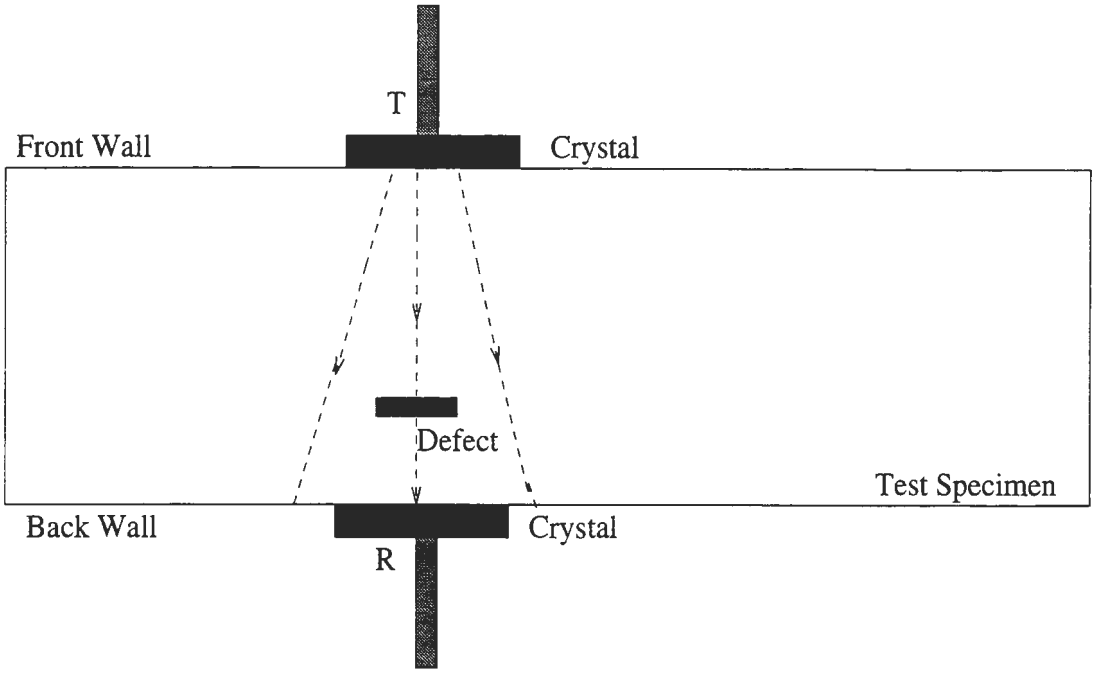

Figure 2.1: Normal pitch-catch technique of ultrasonic testing

One transducer injects (pitches) a sound pulse into the test piece, while the other transducer receives (catches) the transmitted sound. Any inhomogeneity in the path of the beam causes some of the ultrasonic energy to be absorbed or reflected, and the evidence of the existence of the defect is shown as a reduction in the total amount of the energy received at the receiving transducer, remote from the source of the energy. In addition to flaw detection, transmission methods are used to determine grain size, porosity, physical properties and wall thickness measurement.

A major difficulty encountered with the pitch-catch technique, is that in case of presence of bonding of materials in the test specimen, the acoustic transmission properties of the materials vary [4]. The pulse-echo method is better suited for such

applications, and is discussed in the following subsection.

Pulse-echo technique

The pulse-echo technique is the most popular UT testing method and is used most often in industrial ultrasonic flaw detection systems. In the pulse-echo system, an electric pulse is applied to the transmitter probe, which produces a short ultrasonic pulse which is propagated into the specimen through a couplant layer. The same transducer is used as the receiver, since piezo-electric transducer generates mechanical vibrations under electrical stimuli and vice-versa. The transmitted beam is reflected from the opposite surface or the defect back to the transducer as shown in the Figure 2.2.

The pulse-echo technique depends upon the detection of the energy reflected back to its source. For bonded structure, pulse-echo is a better option, since it is more direct than the pitch-catch technique, as the actual reflection from the area under examination is detected and evaluated. Unlike pitch-catch, pulse-echo technique requires access to only one surface of the test specimen, which is an added benefit.

Other techniques

Besides these two main techniques, other methods used for ultrasonic testing are resonance, acoustic imaging and frequency modulation [2].

The resonance technique utilizes the ability of a body to resonate due to artificially induced resonating frequencies. After the "harmonic frequency" has been determined for the reference material, test pieces are subjected to the same frequency or frequency spectrum. The lack of induced vibrations indicates a difference between

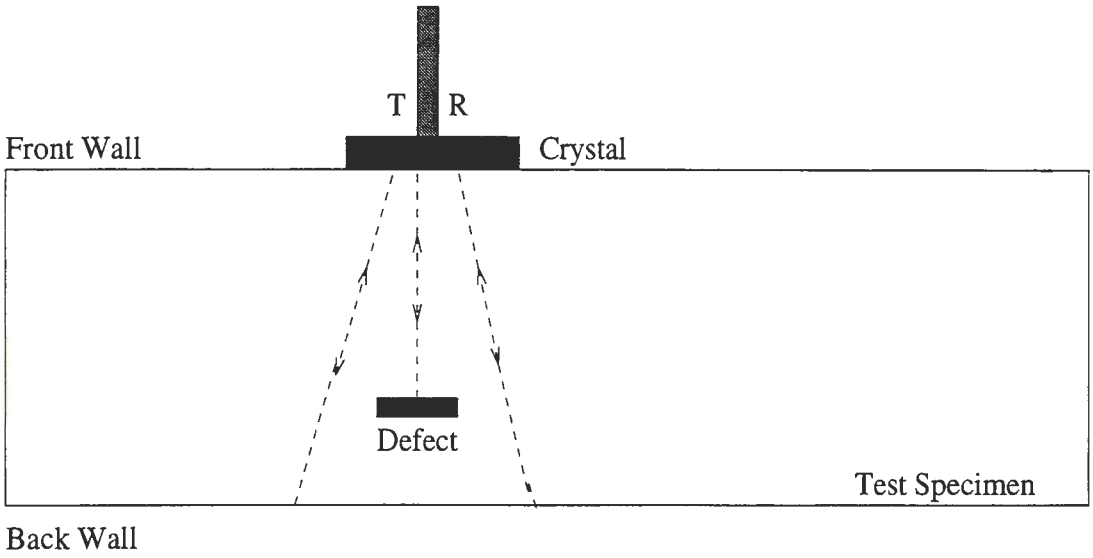

Figure 2.2: Normal pulse-echo technique of ultrasonic testing

the standard and the test piece. Generally, this method of ultrasonic testing is limited to thin sections.

The acoustical imaging technique uses the visual indication of the sound energy transmitted through a test piece. The methods of visualization include special electronic tubes, temperature sensitive compounds, lasers, and television apparatus to "visualize" the test piece.

The frequency modulation method of testing employs one transducer whose frequency is continually varying. Sound is constantly sent and received by the transducer. The ability of the transducer to receive a signal while it is emitting a signal is due to the differences in frequencies of the signal received and the signal being sent.

Modes of Ultrasonic Testing

An additional parameter that is usually varied in ultrasonic testing using either the pulse-echo or pitch-catch mode, is the angle of incidence of the ultrasonic beam into the test specimen. Based on this parameter, there are two modes of operation with each of the two techniques (pulse-echo and pitch-catch), namely normal incidence and angle-beam incidence.

Normal incidence

In normal incidence ultrasonic testing, the ultrasonic beam is induced normal to the major axis of the specimen being tested. It is most effective in flaw characterization where the flaws are mainly parallel to the axis of the unit under test. The discussion in the earlier sections has implicitly assumed a normal incidence mode. Figures 2.1 and 2.2 display normal incidence pitch-catch and pulse-echo modes of testing respectively. Note that normal incidence testing uses longitudinal waves as the sound waves used for flaw characterization.

Angle beam incidence

In order for a reflector to be displayed, the axis of the sound beam must be perpendicular to the reflector. Normal beam transducers are effective only for detecting flaws that are parallel to the test surface. When the largest face of the discontinuity is expected to be at orientations other than parallel to the surface, angle-beam mode is used for flaw detection.

In case of the nuclear pipe weld geometry illustrated in the Figure 1.1, as stated earlier, most of the cracks occur in the vicinity of the weld material, i.e. in the

heat affected zone. A characteristic of the weld material is the granular structure, resulting in scattering of the UT energy. Hence, it is not possible for a transducer to be placed on the weld crown to detect cracks underneath using normally incidence waves. Hence the technique used for ultrasonic testing of welded pipes is angle-beam pulse-echo, which is a standard technique used in the industry.

Angle beams are produced in the test material using the principle of refraction. Refraction is the bending of a sound beam when it passes through an interface between materials of different acoustic velocity. The relationship between the angle of incidence and the angle of refraction is given by Snell's law, stated below

$$\frac{Sin\theta 1}{Sin\theta 2} = \frac{\vartheta 1}{\vartheta 2} \tag{2.6}$$

where $\theta 1$ is the angle of incidence, $\theta 2$ is the angle of refraction, $\vartheta 1$ is the velocity of sound in the incident medium an $\vartheta 2$ is the velocity of sound in the refracted medium. The angle of refraction depends upon, both the incident angle and the ratio of acoustic velocities through which the incident and refracted beams are travelling. As the angle of the incident beam increases, the angle of the refracted beam also increases. At a critical angle, the refracted beams are refracted 90^0, and are in effect, fully reflected within the first material. This is called as the first critical angle, and only the shear component of the refracted beam is transmitted to the second material. The second critical angle is the incident angle that causes the refracted shear beam to be refracted 90^0.

One of the most commonly used technique, for angle beam generation is the use of a suitable angle wedge, to launch the beam into the specimen, at the required angle. Typical angles for angle-beam incidence is the $30^0 - 60^0$ range.

Figure 2.3 shows angle-beam pitch-catch mode while Figure 2.4 shows angle-

beam pulse-echo mode of ultrasonic testing.

Ultrasonic Imaging

The basic concepts underlying the imaging techniques using ultrasound are discussed in this section. The images produced by ultrasonic waves represent the internal interaction with the mechanical properties of defects and other features in material, and hence, serve as a powerful tool in modern NDT research [5]. This section is intended to cover some of the imaging methodologies involved in the application of defect characterization.

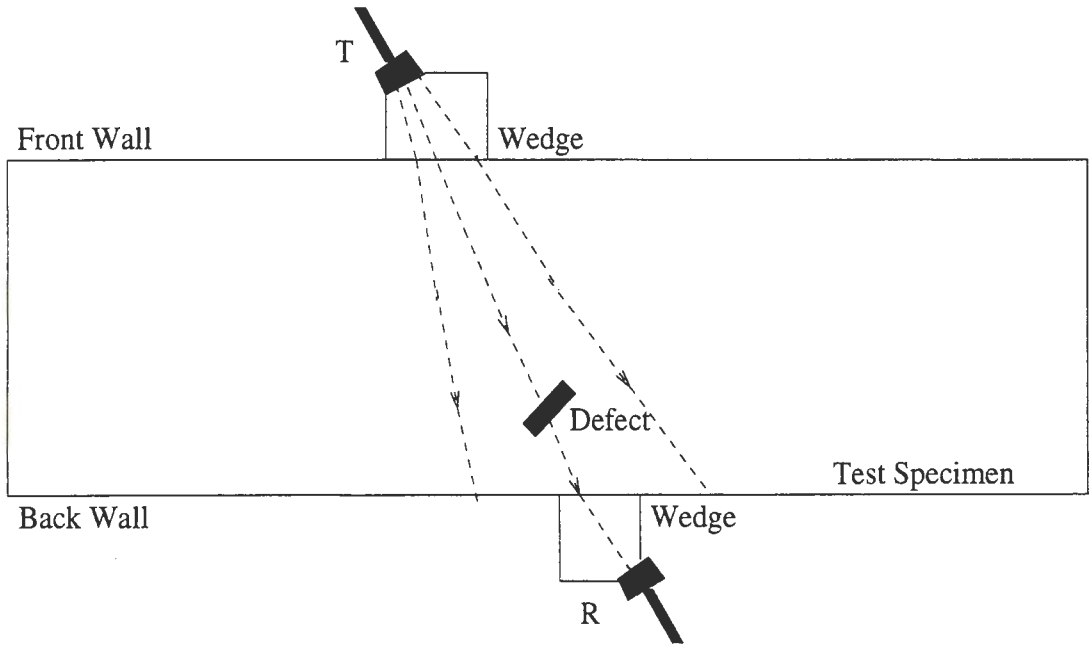

Figure 2.3: Angle-beam pitch-catch technique of ultrasonic testing

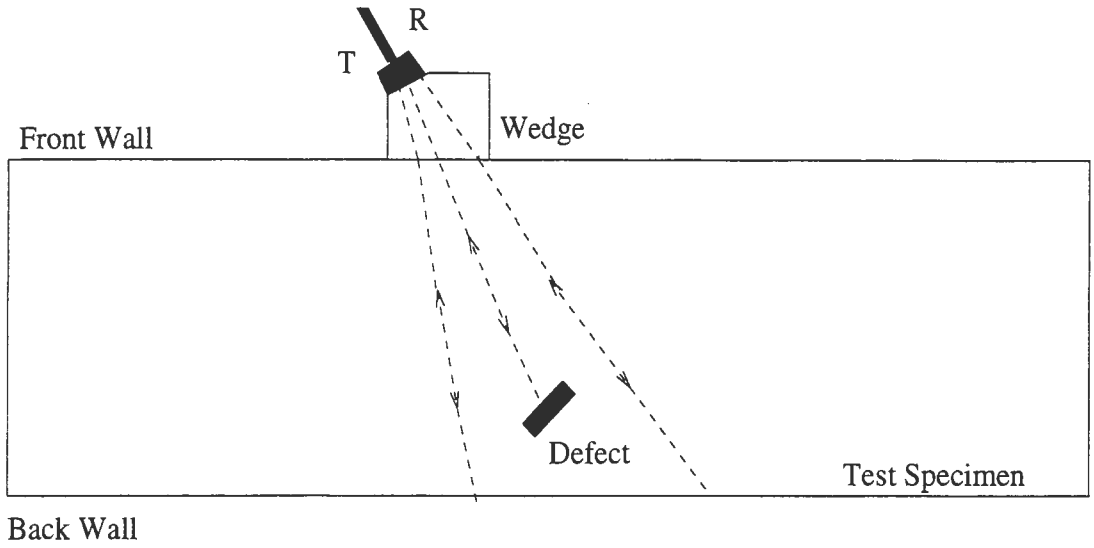

Figure 2.4: Angle-beam pulse-echo technique of ultrasonic testing

A-Scan

There are several ways in which received signals can be displayed in order to extract the necessary information describing any particular medium, during a typical ultrasonic test.

Ideally the display signal represents the reflectivity of the work piece, as a function of time, where time is a measure of the depth into the specimen [9]. This display of the reflectivity as a function of time is most commonly used and is referred to as the A-scan signal.

A typical A-scan of a stainless steel pipe being scanned, using the angle-beam, pulse-echo technique is shown in Figure 2.5. The largest pulse at the left-hand side

corresponds to the front wall echo of the sample and the successive blips correspond to the echoes emanating from defects. The amplitude of these echoes is generally proportional to the size of the reflecting surface, but is also affected by the attenuation effects introduced by both the traveled distance and the inherent composition of the material itself. The A-scan is quite often used to determine the location of the reflector, using the time of flight (TOF), and the velocity of sound in the medium.

For instance, consider the flaw in the sample whose A-scan is displayed in Figure 2.5. The A-scan has been obtained using angle-beam pulse-echo technology in a stainless steel pipe. The angle of incidence θ of the beam is 43^0 and the velocity ν of sound in stainless steel is 0.11 inches/μsecond. The corresponding geometry is shown in the Figure 2.6. In Figure 2.5, the x-axis represents the time of flight, and the y-axis represents the amplitude of the reflected signal. The time of flight (TOF) corresponding to the maximium amplitude in the reflected signal is 29 μs.

The depth d of the flaw from the scanning surface can be calculated using

$$d = TOF\nu \cos\theta \tag{2.7}$$

For the given A-scan this value comes to 2.33 inches below the top surface which is indeed the location of the flaw

B-Scan

The B-scan takes the same signals received in the A-scans and presents them in a different pattern. It displays the reflectivity of a two dimensional slice through a portion of the structure [10].

This format enables the recording of a defect location within a material. The

CHAPTER 3. SAFT

Ultrasonic testing technique is used extensively because of its ability to penetrate thick specimen, to locate the exact location of a flaw, and to detect minute flaws under appropriate conditions. However, there is excessive noise in the reflected signals from grain boundaries and discontinuities in the geometry. Many signal processing techniques have been developed over the years for enhancing the signal to noise ratio of UT signals. This chapter describes the synthetic aperture focusing technique (SAFT), which is used extensively in radar and ultrasonic NDE for image enhancement.

Synthetic-aperture Fundamentals

Synthetic-aperture focusing refers to a process in which the focal properties of a large aperture focused transducer are simulated, by a series of measurement made using a small aperture transducer scanning over a large area. Synthetic-aperture imaging can realize the theoretical resolution potential of ultrasonic waves, improve the signal to noise ratio of the image, and take into account such complex material interactions as irregular refractive interfaces and the complex angular scattering of ultrasonic waves by a defect [11]. The synthetic-aperture method accomplishes these tasks by extensive processing of the data from an ultrasonic transducer, in order to

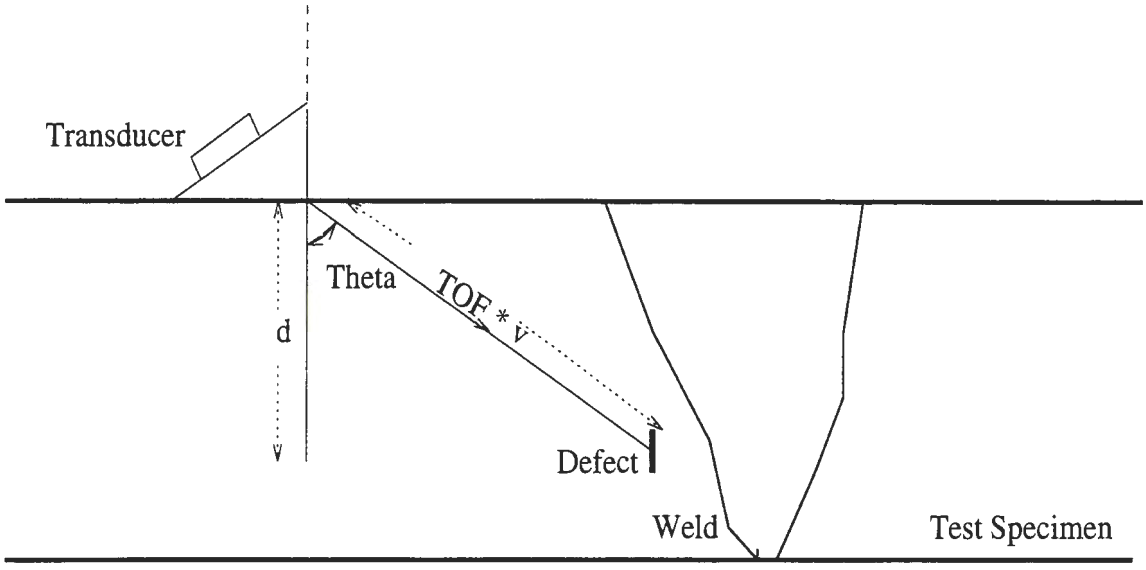

Figure 2.6: Geometry for the flaw depth calculation

abundantly, due to the intrinsic nature of the SAFT algorithm to work on a collection of A-scans at a time.

C-Scan

The C-scan presentation is a plan view of the part under test, and a flaw is indicated in a manner similar to an X-ray of the specimen. In a C-scan, corresponding to a time slice of a region, the image pixel intensity is obtained by observing the peaks in the time slice of the scanned A-scans. The method of raster scanning of a sample is illustrated in Figure 2.9. A typical C-scan of the same pipe, whose A-scan and B-scan are illustrated in Figure 2.5 and 2.8 respectively, is illustrated in Figure 2.10.

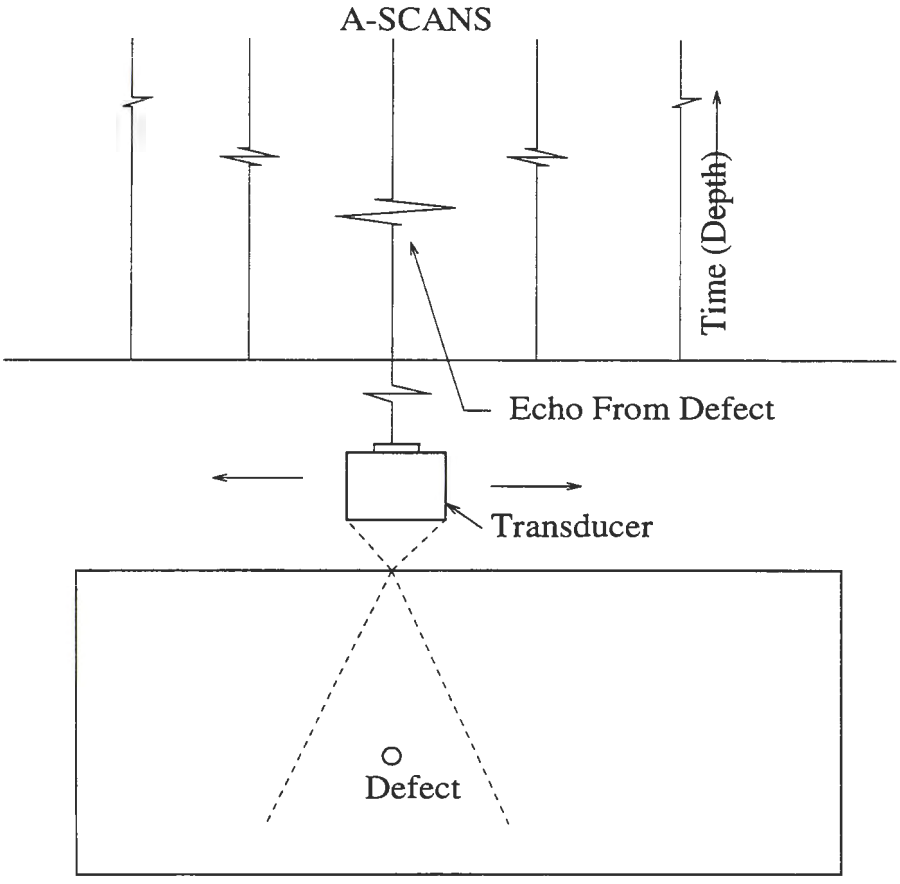

Figure 2.7: B-scan imaging system

Accurate flaw depth cannot be determined from the C-scan presentation, although the flaw sizing in the two dimension can be observed.

Data Storage Issues

An important issue relevant to NDE in general and UT NDE in particular, is the storage and processing of huge amounts of data. Currently, most of the data is digitized and stored on computer-supported storage devices. These are mainly in the

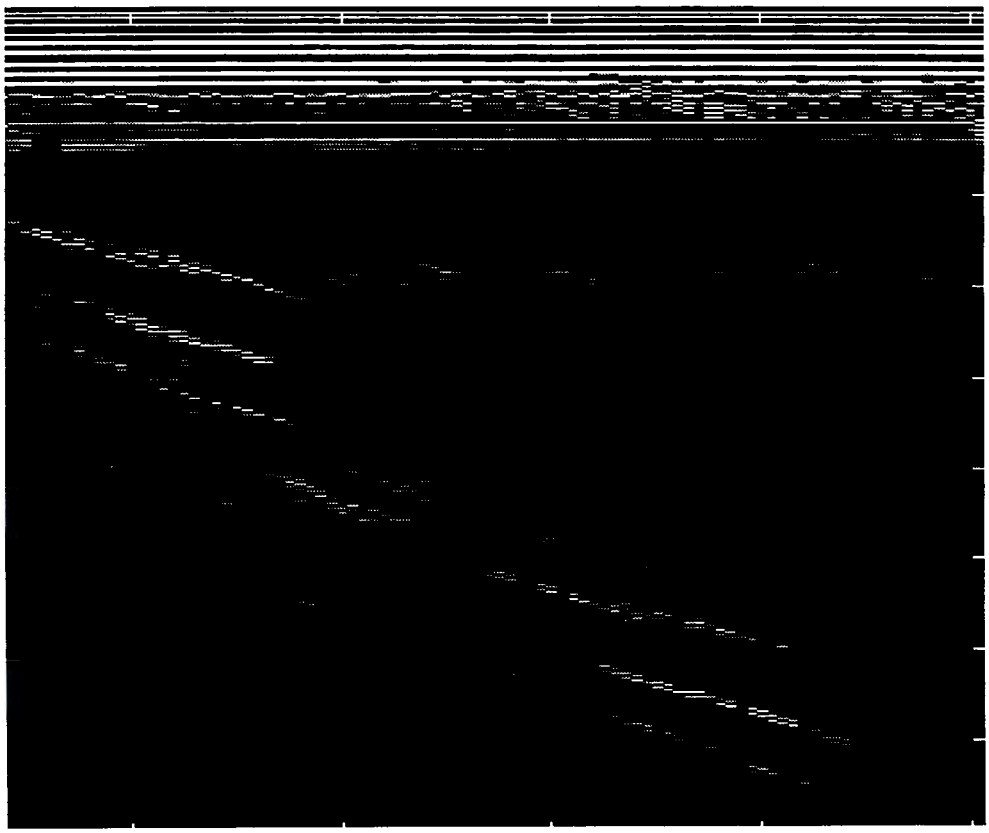

Figure 2.8: B-scan

form of floppy disks, hard drives and tape drives. A typical setup in which a 10" by 3" region of a pipe is scanned using a 2 MHz transducer, and then sampled at 25 mega-samples/second may lead to data files, as large as 100 Mbytes each. This slows down the entire process of performing the subsequent signal processing on the data, and hence it would be beneficial to the industry if real-time techniques are developed using dedicated hardware resources for performing the signal processing in hardware, instead of software.

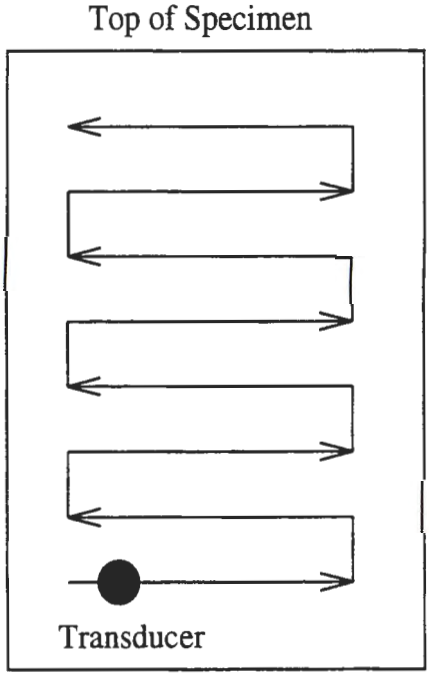

Figure 2.9: Raster scanning of the test specimen

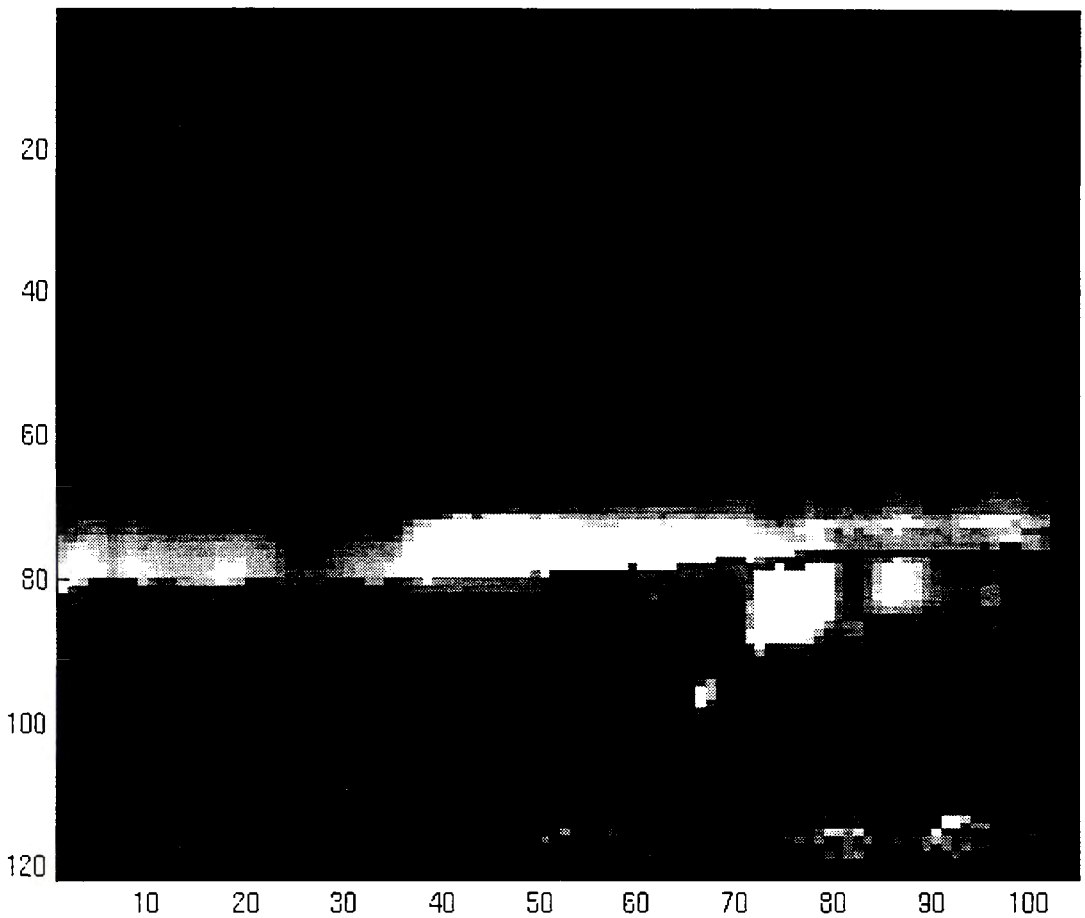

Figure 2.10: C-scan

CHAPTER 3. SAFT

Ultrasonic testing technique is used extensively because of its ability to penetrate thick specimen, to locate the exact location of a flaw, and to detect minute flaws under appropriate conditions. However, there is excessive noise in the reflected signals from grain boundaries and discontinuities in the geometry. Many signal processing techniques have been developed over the years for enhancing the signal to noise ratio of UT signals. This chapter describes the synthetic aperture focusing technique (SAFT), which is used extensively in radar and ultrasonic NDE for image enhancement.

Synthetic-aperture Fundamentals

Synthetic-aperture focusing refers to a process in which the focal properties of a large aperture focused transducer are simulated, by a series of measurement made using a small aperture transducer scanning over a large area. Synthetic-aperture imaging can realize the theoretical resolution potential of ultrasonic waves, improve the signal to noise ratio of the image, and take into account such complex material interactions as irregular refractive interfaces and the complex angular scattering of ultrasonic waves by a defect [11]. The synthetic-aperture method accomplishes these tasks by extensive processing of the data from an ultrasonic transducer, in order to

encode the resulting image information in such a manner, that the necessary human interpretation can be done faster and more easily.

Ultrasonic images can contain, and effectively convey, an extremely large amount of information. It is widely accepted among researchers that the ultrasonic pulse returned from a test sample contains much more information about the interaction between the ultrasound and the material, than is commonly extracted from conventional displays. The more adept practitioners of the ultrasonic art can either consciously or unconsciously make use of this wealth of information. The presence of such adept operators is encouraging to those researches attempting to extract more information from the ultrasonic signal, as it implies the existence of the data they desire, but it is discouraging to those managers wishing to employ ultrasonic testing on a routine basis, as it promises inconsistent results over time and with different personnels. SAFT is able to enhance the images, so that it is possible for many more people to reliably interpret the ultrasonic signals [11].

The synthetic-aperture technique utilizes the information in the ultrasonic data to produce high quality images. The SAFT process presents the available data in an image format that is much easier to interpret. The concept of synthetic-aperture imaging is borrowed from radar (microwave) imaging techniques of the same name. While there are significant differences between the ultrasonic and the microwave implementation, there is a commonality in concepts and motivation, since the wave physics of radar antenna and ultrasonic transducer is quite similar. The designers of both, ultrasonic transducer and air borne radars, realized that there were practical limits to their ability to fabricate the large antenna or transducers required to form high resolution images. The solution in both fields is to move a small transducer

in such a manner that the collected data can be later processed, to simulate the desired large transducer. This processing, in effect, synthesizes the physical processes occurring in a large, but unobtainable, aperture transducer and thus is referred to as synthetic-aperture imaging

In both, ultrasonic and radar, the data are focussed, not by some physical mechanism employed during data acquisition, such as a curved transducer, but by subsequent data processing. Since this data processing is done in software, it offers considerable advantages in terms of flexibilty and evaluation, as against varying the focii of the transducers physically to image different parts.

Both ultrasound and radar synthetic-aperture techniques explicitly make use of both the amplitude and the phase information contained in their respective signals. Synthetic-aperture ultrasonic images are formed from RF wave forms, and the ultrasonic phase information manifested in the processed image through the mechanism of constructive and destructive interference, plays an important role, in the subjective improvement of the ultrasonic image [11].

Quantitative Interpretation of SAFT

Digital ultrasonic imaging can be viewed as collection of ultrasonic data followed by processing of the data by an algorithm which represents the ultrasonic scattering information in an image. This section presents the theoretical development of the ultrasonic defect characterization and the resulting SAFT processing.

Quantitative interpretation of ultrasonic images requires careful investigation and understanding of the inverse scattering scheme under consideration [12]. The

in such a manner that the collected data can be later processed, to simulate the desired large transducer. This processing, in effect, synthesizes the physical processes occurring in a large, but unobtainable, aperture transducer and thus is referred to as synthetic-aperture imaging

In both, ultrasonic and radar, the data are focussed, not by some physical mechanism employed during data acquisition, such as a curved transducer, but by subsequent data processing. Since this data processing is done in software, it offers considerable advantages in terms of flexibilty and evaluation, as against varying the focii of the transducers physically to image different parts.

Both ultrasound and radar synthetic-aperture techniques explicitly make use of both the amplitude and the phase information contained in their respective signals. Synthetic-aperture ultrasonic images are formed from RF wave forms, and the ultrasonic phase information manifested in the processed image through the mechanism of constructive and destructive interference, plays an important role, in the subjective improvement of the ultrasonic image [11].

Quantitative Interpretation of SAFT

Digital ultrasonic imaging can be viewed as collection of ultrasonic data followed by processing of the data by an algorithm which represents the ultrasonic scattering information in an image. This section presents the theoretical development of the ultrasonic defect characterization and the resulting SAFT processing.

Quantitative interpretation of ultrasonic images requires careful investigation and understanding of the inverse scattering scheme under consideration [12]. The

increasingly difficult. One might wish to recover information by variation of the transmitting transducer, $\vec{R_O}$, so that information from all possible points is made available to the receiving transducer.

Variation of $\vec{R_O}$, however does not extract all the information available, and it would definitely be better if the receiving transducer, $\vec{R}$, could be synthetically increased, using the variations of $\vec{R_O}$. Synthetic aperture focusing technique is a highly successful imaging scheme, which is based on the observation that there is a scattering of amplitude travel-time wavefronts from the defects [13] [14]. The goal of SAFT is to back-propagate these wavefronts to the scattering defect where they came from. This is achieved implying the following assumptions:

1. The wavefronts are essentially treated as scalar wavefields; hence $\vec{\phi_i}$ becomes ϕ_i and $\vec{\phi_s}$ becomes ϕ_s.

2. The incident wavefield is supposed to emanate from a point source located at R_O.

3. The defect is decomposed into single non-interacting scatterers, which act as point sources after illumination with the incident wavefield.

4. The incident pulse is assumed to be 'nearly' infinitely broad-band, i.e. its time structure is represented by $F(t)$, where $F(t)$ denotes a very sharp nearly δ-like impulse.

In the following sub-section we describe briefly how these assumptions lead to the formulation of the imaging SAFT algorithms.

important parameters of an ultrasonic scattering experiment are the mode of operation, be it either pulse-echo or pitch-catch, as well as the bandwidth of the transmitted pulse. For imaging purposes, the scattered wavefield has to be observed at a considerable number of spatial points within a synthetic aperture.

Let us denote the the position of the transmitting transducer by the spatial vector $\vec{R_O}$ and that of the receiving transducer by $\vec{R}$. Let us call the incident wave field $\vec{\phi_i}$ and the observable scattered field as $\vec{\phi_s}$. Now $\vec{\phi_s}$ is a function of ($\vec{\phi_i}$, $\gamma(\vec{R'})$, $\vec{R_O}$, $\vec{R}$, t) where t is the time and $\gamma(\vec{R'})$ is a description of the geometry of the material defect, which is defined as follows

$$\begin{aligned} \gamma(\vec{R'}) &= 1 \qquad \vec{R'} \quad inside\ the\ defect \\ &= 0 \qquad \vec{R'} \quad outside\ the\ defect \end{aligned} \tag{3.1}$$

The following relations have been developed assuming that the defect resides in a linear, isotropic and homogeneous material. Now, assuming that $\vec{\phi_i}$ is a short broad band pulse, then data collection implies the observation and digital storage of $\vec{\phi_s}$ as a function of the receiving transducer $\vec{R}$ and the time t [12]. Consequently, an RF data field is obtained, which supplies us with information to be exploited for imaging purposes.

It is intuitively clear that confining the receiving transducer $\vec{R}$ to a spatially limited region and restricting the frequency bandwidth of the incident pulse results in a deterioration of the image quality, depending upon the complexity of the defect geometry $\gamma(\vec{R'})$. Stated in simple terms, this means that we would like the receiving transducer (aperture) to be as large as possible. However, because of the manufacturing limitations on the size of the transducer, it is not feasible to increase the size beyond a certain limit. Therefore, quantitative nondestructive evaluation becomes

increasingly difficult. One might wish to recover information by variation of the transmitting transducer, $\vec{R_O}$, so that information from all possible points is made available to the receiving transducer.

Variation of $\vec{R_O}$, however does not extract all the information available, and it would definitely be better if the receiving transducer, $\vec{R}$, could be synthetically increased, using the variations of $\vec{R_O}$. Synthetic aperture focusing technique is a highly successful imaging scheme, which is based on the observation that there is a scattering of amplitude travel-time wavefronts from the defects [13] [14]. The goal of SAFT is to back-propagate these wavefronts to the scattering defect where they came from. This is achieved implying the following assumptions:

1. The wavefronts are essentially treated as scalar wavefields; hence $\vec{\phi_i}$ becomes ϕ_i and $\vec{\phi_s}$ becomes ϕ_s.

2. The incident wavefield is supposed to emanate from a point source located at R_O.

3. The defect is decomposed into single non-interacting scatterers, which act as point sources after illumination with the incident wavefield.

4. The incident pulse is assumed to be 'nearly' infinitely broad-band, i.e. its time structure is represented by $F(t)$, where $F(t)$ denotes a very sharp nearly δ-like impulse.

In the following sub-section we describe briefly how these assumptions lead to the formulation of the imaging SAFT algorithms.

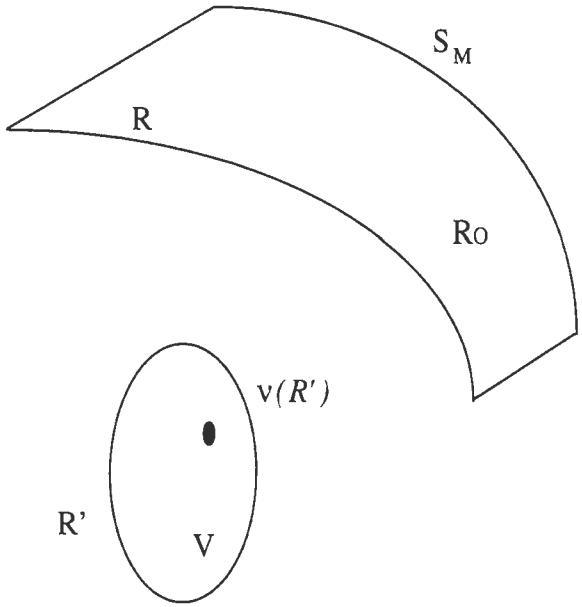

Figure 3.1: Scattering object and measuring surface

The 'inversion' of the Equation 3.6, i.e. the determination of $\gamma(R')$ through the knowledge of $\phi_s(R,t)$ can be achieved, recognizing the fact that every single point scattered, for example R_s, contributes linearly to the scattered field [12].

$$\phi_s^{R_s}(R,t) = \frac{F(t - \frac{|R_s - R_O|}{c} - \frac{|R_s - R|}{c})}{|R_s - R_O||R_s - R|} \tag{3.7}$$

where R is varied along the measurement surface S_M by some appropriate procedure.

Due to the sharpness of the impulse $F(t)$, $\phi_s^{R_s}(R,t)$ is significantly non-zero only for times

$$t_s(R) = \frac{|R_s - R_O|}{c} + \frac{|R_s - R|}{c} \tag{3.8}$$

Intuitively, $t_s(R)$ corresponds to the time when the incident wavefront from R_O

Time domain back-propagation of wavefronts: SAFT

Figure 3.1 gives a geometrical illustration of the scattering objects and the measurement surface. Suppose the transmitting transducer is modeled as a scalar point source R_O on a measurement surface S_M, transmitting the impulse $F(t)$. The incident field at the point R' is then given by

$$\phi_i(R_O, R', t) = \frac{F(t - \frac{|R'-R_O|}{c})}{|R' - R_O|} \tag{3.2}$$

where c is the wave velocity in the medium.

The material inhomogeneity represented by the defect, and its illumination by the incident field, gives rise to an induced source $\phi_B(R_O, t)$ which is responsible for the scattered field. The entire defect volume V enclosed by $\gamma(R')$ can be represented by the scattered field equation

$$\phi_s(R, t) = \int\int_v\int \frac{\phi_B(R', t - \frac{|R'-R|}{c})}{|R' - R|} d^3R' \tag{3.3}$$

Now as per the third assumption, ϕ_B is modeled as a superposition of independent point sources, hence

$$\phi_B(R', t) = \gamma(R')\phi_i(R_O, R', t) \tag{3.4}$$

Therefore the scattered field becomes

$$\phi_s(R, t) = \int\int_{-\infty}^{\infty}\int \frac{\gamma(R')\phi_i(R_O, R', t - \frac{|R'-R|}{c})}{|R' - R|} d^3R' \tag{3.5}$$

Using [3.2] for ϕ_i,

$$\phi_s(R, t) = \int\int_{-\infty}^{\infty}\int \frac{\gamma(R')F(t - \frac{|R'-R|}{c} - \frac{|R'-R_O|}{c})}{|R' - R||R' - R_O|} d^3R' \tag{3.6}$$

reaches R_s and then to R.

A reconstruction of the defect geometry point R_s, given by $\gamma(R_s)$ can therefore be defined by integrating $\phi_s^{R_s}(R,t)$ along the measurement surface S_M, with respect to R, for exactly the points defined by Equation 3.8. All contributions of the point scatterer are summed up. It is intuitively clear that the point $R' \neq R_s$ receives a much smaller amplitude from $t_s(R)$ because the curve,

$$t'(R') = \frac{|R' - R_O|}{c} + \frac{|R' - R|}{c} \tag{3.9}$$

has only one point in common, namely $(R' = R_s)$, with equation 3.8.

Accounting for every point scatterer within $\gamma(R')$, the defect can be reconstructed as

$$\gamma(R') = \int\int_{S_M} \phi_s(R, t'(R'))|R' - R_O||R' - R|\, d\Omega \tag{3.10}$$

The integration is with respect to the surface elements on S_M.

Qualitative Analysis of SAFT

As has been stated in earlier sections, SAFT refers to a process in which the focal properties of a large-aperture focused transducer are synthesized by a series of measurements, made using a small-aperture transducer, that scans a large area [15]. In other words, SAFT is the process of simulating a focused transducer.

SAFT has several advantages over physical focusing techniques. SAFT has a great deal of flexibility in data collection and image formation [16]. If a test object of irregular size and shape has to be inspected, the data can be processed in a way that minimizes the error caused by refraction. To make a similar correction with a

physical focus system would require a transducer with different focal properties to be designed for every different part to be inspected [16].

In case of the nuclear pipe UT inspection technique, a small contact transducer is positioned on the test specimen. It simulates a "point" transmitter-receiver, and a broad divergent ultrasonic beam is launched into the object. As the transducer is scanned over the surface of the object, a series of amplitude v/s time A-scans are recorded for each position of the transducer. Every reflector produces a collection of echoes in the A-scan records. The locus of each elementary reflector produces a characteristic hyperbolic curve, in a set of linear positions, as shown in Figure 3.2.

The apex and curvature of the hyperbola are completely determined by the depth o f the reflector within the test object. This deterministic relationship between the echo location in the recorded A-scans and the location of the reflectors wit hin the test object makes it possible to generate a processed image from the new data by the coherent summation process [16].

If the scanning and surface geometries are known, it is possible to accurately predict the shape of the locus of echoes for each point within the test object. The process of coherent summation involves shifting the raw A-scans by the predicted time-delay and summing of the shifted echo data. The time-compensated A-scans are then averaged over a number of positions, which is the aperture size. The aperture of the synthesized transducer is the number of A-scans that are coherently summed in SAFT. For all processing purposes, the aperture can be treated as a window into the collection of A-scans. The time-shifting is done with respect to the A-scan which is at the center of the aperture (COA). Following the averaging, the resultant vector is placed at the center of the chosen aperture.

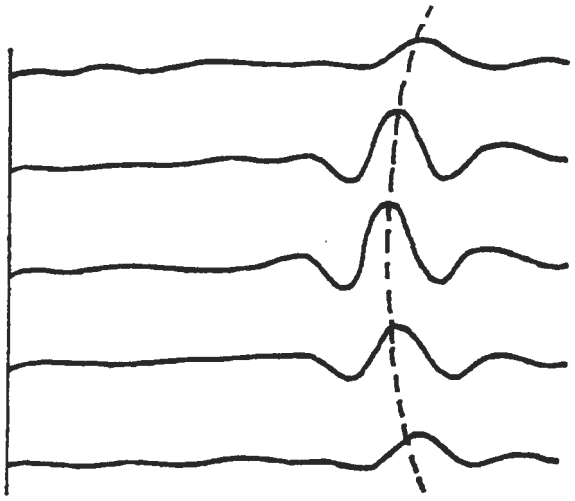

Figure 3.2: Hyperbolic reflections from the same reflector in different A-scans

If the point being imaged corresponds to a reflection from a defect, or in other words, correlates with a locus of A-scan echoes, then all of the A-scans will add in phase during the process of spatial averaging to produce a well-defined signal. This is illustrated in Figure 3.3. However, if the point being imaged, corresponds to noise, or in other words does not correlate with a locus of A-scan echoes, then destructive interference of the A-scans will take place, and the spatial average will be nearly zero. Figure 3.4 illustrates this destructive interference. Thus, there is both an improvement in signal level and a reduction on noise level producing an image with a high signal to noise ratio. It should be noted that the SAFT procedure is performed at a specific depth site in the specimen under test.

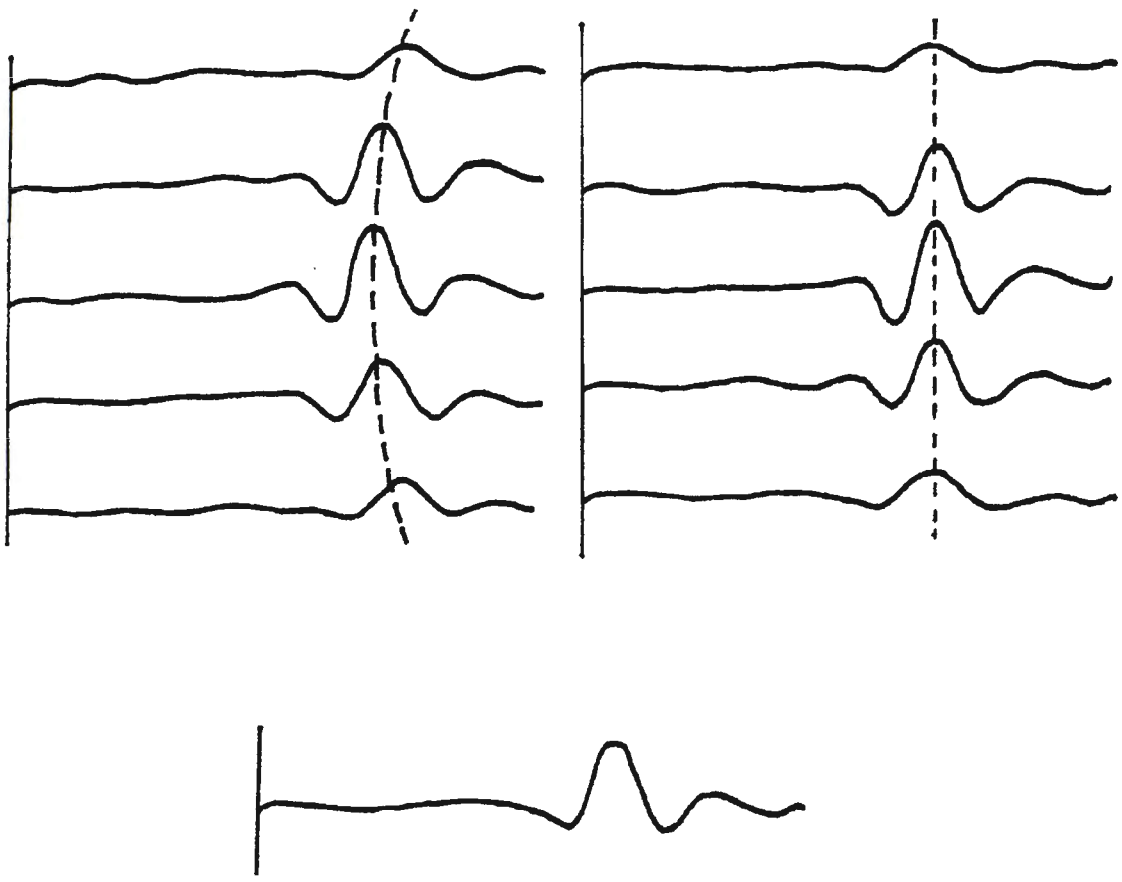

Figure 3.3: Constructive interference during SAFT

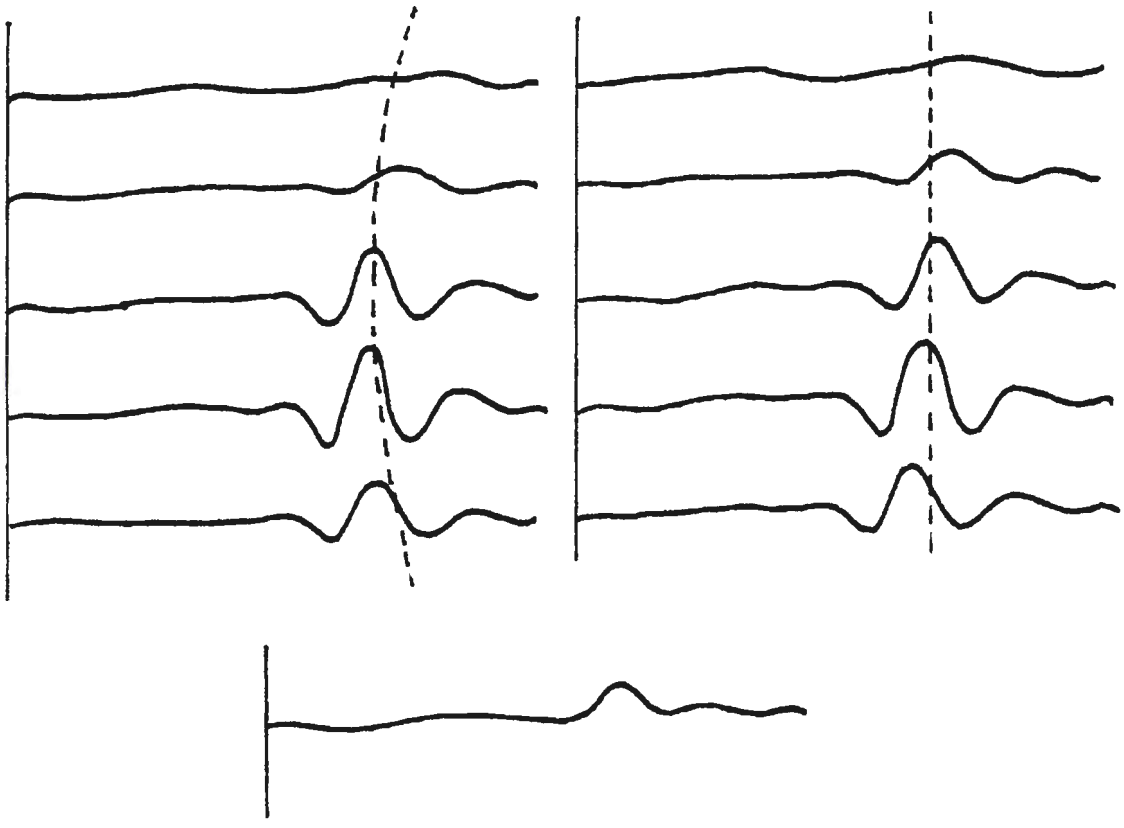

Figure 3.4: Destructive interference during SAFT

CHAPTER 4. ANGLE BEAM SAFT

Angle Beam Theory

In order for a reflector to be displayed, the axis of the sound beam must be perpendicular to the reflector. Straight beam transducers are effective only for reflectors that are parallel to the test surface. When the largest face of the discontinuity is expected to be at an orientation, other than parallel to the surface, angle beam transducers are used to aim the axis of the beam perpendicular to the discontinuities.

There are different ways of introducing angle beams into the test material, depending on the coupling technique used. In order for the angle beams to be produced in the test material, the transducer's beam axis must be aimed towards the test surface at an angle. Contact testing employs angle wedges, immersion testing permits continuously variable angulation of the transducer by means of an adjustable manipulator assembly.

Angle beams are produced in the test material using the principles of refraction. Refraction is the bending of a sound beam when it passes through an interface between materials of different acoustic velocity. The transducer is aimed so as to direct the beam towards the test material interface at an angle.

When a sound beam is incident to an interface at an angle other than 90^0, as illustrated in Figure 4.1, a phenomenon called mode conversion occurs. In addition

to the simple reflected beam, a portion of the incident beams energy converts at the interface to a beam with a different mode of vibration, and reflects at an angle other than the angle of incidence (or reflection).

When sound refracts, there is mode conversion, too. Thus, there is an additional refracted beam which is a mode conversion of the incident beam.

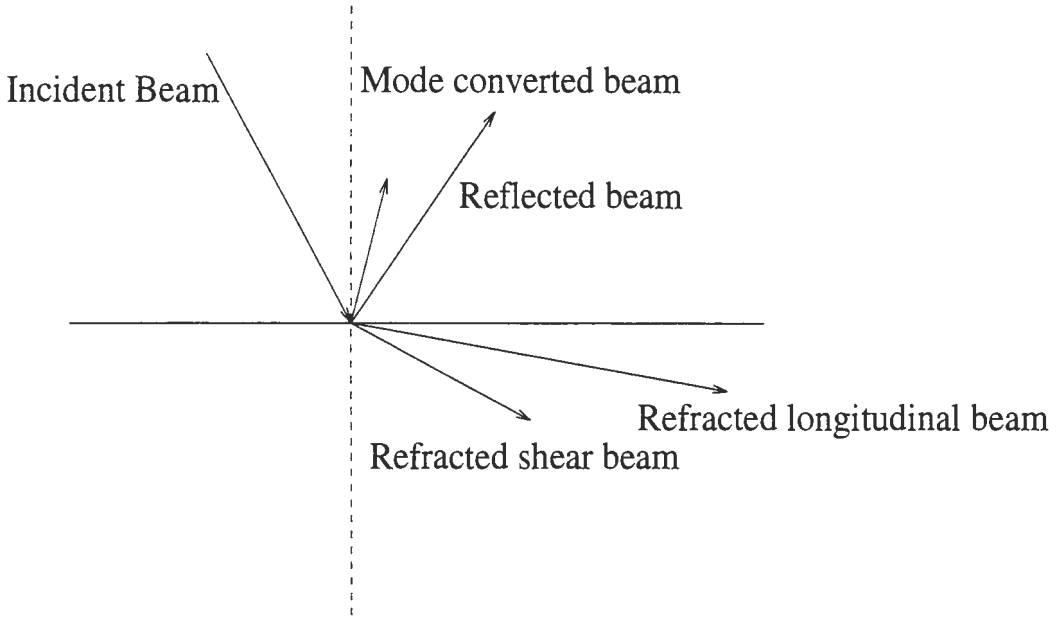

Figure 4.1: Mode conversion of sound waves

As the angle of the incident beam increases, the angle of the refracted beams also increases. At a critical angle, the longitudinal refracted beams is refracted 90^0, and is in effect, fully reflected within the first material. This is called as the first critical angle and only the shear component of the refracted beam is transmitted to the second material as illustrated in Figure 4.2. The second critical angle is the

incident angle that causes the refracted shear beam to be refracted 90^0. For example, with a plastic wedge producing angle beams in carbon steel, the first critical angle is 27.2^0 and the second critical angle is 55.8^0.

In the experiments conducted, the data has been collected from stainless steel pipes, using plastic wedges, so that the angle of refraction is 43^0. The shear waves dominate in this particular testing setup.

Relevant Issues with Angle Beam Mode of Scanning

Three of the most important issues which distinguish and complicate angle-beam SAFT from normal-beam SAFT are discussed below.

1. Multiple Sound paths

   In case of angle-beam pulse-echo mode of inspection, with finite depth of material, multiple sound paths can contribute to the processed image.

   There are three paths that can contribute reflection echoes in the data. These paths are shown in Figure 4.3. One needs to be aware of the physics of the situation to avoid misinterpreting images or to use the multiple path information to build greater accuracy into the final image. In Figure 4.3, the material is of thickness T, and the defect of interest is located at $x = 0$ and at a depth D in the material [16]

   - The first path is the direct back-scattered path ($P_1 - P_1$) from the sound field entrance into the part to the defect and back to the receiver. Analysis shows that the data along this path will be deterministic, that is, one unique object depth corresponds to one unique hyperbolic curve. This

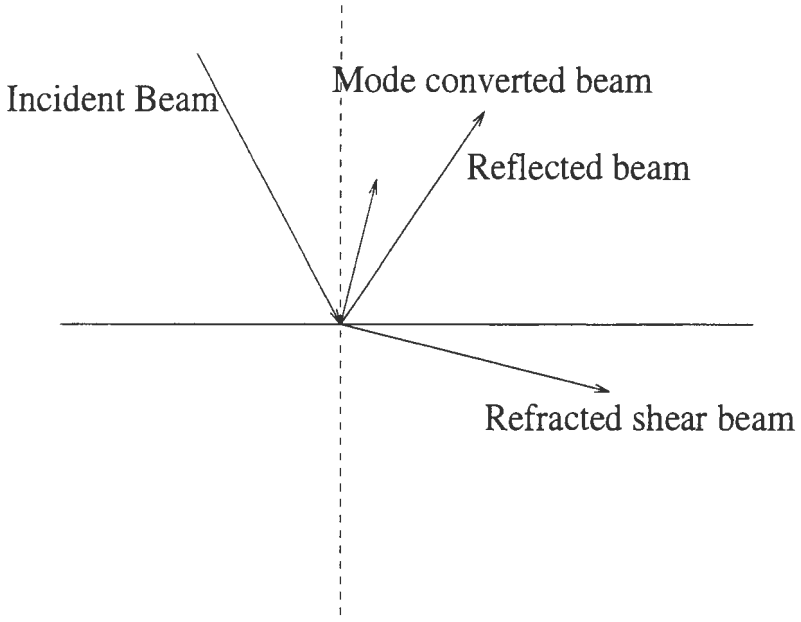

Figure 4.2: Angle of incidence is greater than the first critical angle

curve is defined by the equation

$$F(x, D) = \sqrt{D^2 + X^2} \tag{4.1}$$

- The second sound path is $(P_2 - P_3 - P_1)$ from the sound field entrance point of the part, to the back surface, to the defect and finally to the receiver. The sound path is the sum of the length of the ray paths P_1, P_2 and P_3. The equation for the corresponding curve is

$$F(x, D, T) = \sqrt{(D^2 + X^2)} + \sqrt{(2T - D)^2 + X^2} \tag{4.2}$$

This path is identical to the reverse sequence of $(P_1 - P_3 - P_2)$. This path contributes a very large return echo since it relies on the strong forward-

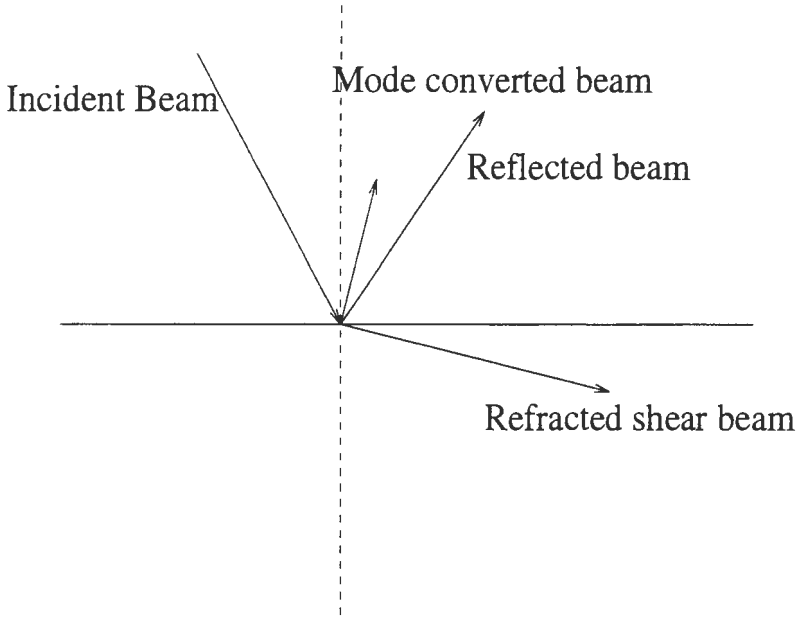

Figure 4.2: Angle of incidence is greater than the first critical angle

curve is defined by the equation

$$F(x, D) = \sqrt{D^2 + X^2} \tag{4.1}$$

- The second sound path is $(P_2 - P_3 - P_1)$ from the sound field entrance point of the part, to the back surface, to the defect and finally to the receiver. The sound path is the sum of the length of the ray paths P_1, P_2 and P_3. The equation for the corresponding curve is

$$F(x, D, T) = \sqrt{(D^2 + X^2)} + \sqrt{(2T - D)^2 + X^2} \tag{4.2}$$

This path is identical to the reverse sequence of $(P_1 - P_3 - P_2)$. This path contributes a very large return echo since it relies on the strong forward-

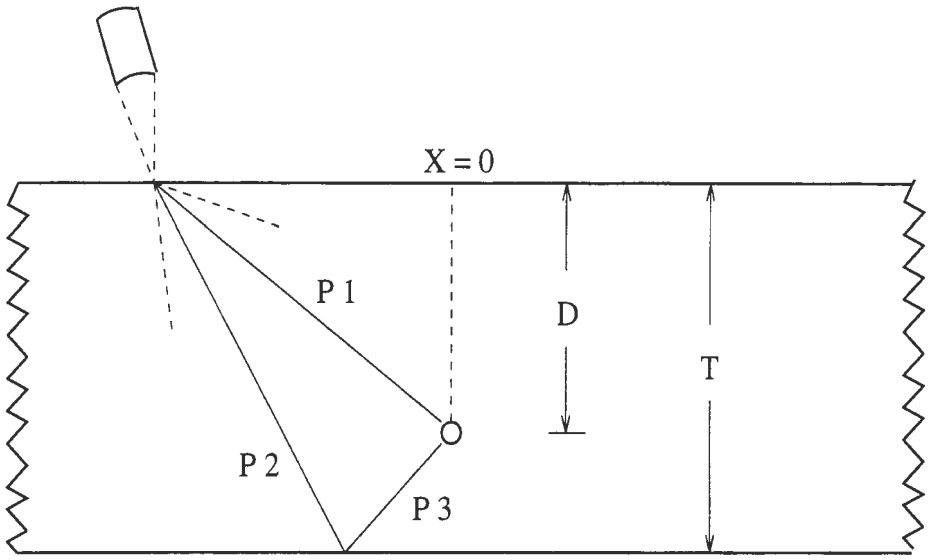

Figure 4.3: Multiple sound paths in angle-beam pitch-catch mode of ultrasonic testing

scattered signal rather than the weaker-back scattered signal [16].

- The third sound path to be considered is from the sound field entrance point on the part, to the back surface, to the defect, back-scatter from the defect to the back surface and return to the receiver or $(P_2 - P_3 - P_3 - P_2)$. This path forms the mirror image of the defect and back relies on the usually weak back scattered signal. The equation for the corresponding curve is

$$F(x, D, T) = \sqrt{(2T - D)^2 + X^2} \tag{4.3}$$

Depending on the defect type, orientation and other characteristic, one of the three paths will dominate the recorded experimental data. The general-purpose SAFT algorithms is capable of constructing all three of the propagation paths for angle-beam data.

2. Periodicity

An interesting phenomenon involving angle-beam scanning is that the same flaw is seen from two transducer position that are a full V-apart. This is illustrated in Figure 4.4. A half-V corresponds to the time required for the beam to travel an entire depth of the specimen. A full-V is the summation of two half Vs. This periodicity of the flaw in the A-scan records occurs since, during the angular travel of the beam, it gets reflected from the front and the back wall surfaces. Thus when the transducer is at position T_1, the beam path to the defect is $P_1 - d - P_1$. When the transducer is at T_2, which one full-V away from T_1, the sound path is $P_3 - P_2 - P_1 - d - P_1 - P_2 - P_3$. Note that for T_2, because of the longer path, the reflection in the A-scan occurs later. Also, the amplitude of reflection from the defect in case of T_2 is smaller, because of the higher attenuation due to the longer path.

A typical B-scan in which this periodicity is exhibited is shown in the Figure 4.5. The A-scans have been plotted vertically. As can be seen, the same defect is seen multiply in the upper left hand side and the lower right hand side. The difference in their time of flights and amplitudes can also be seen.

3. Ellipsoidal Incidence

An additional complication encountered while performing angle-beam SAFT is

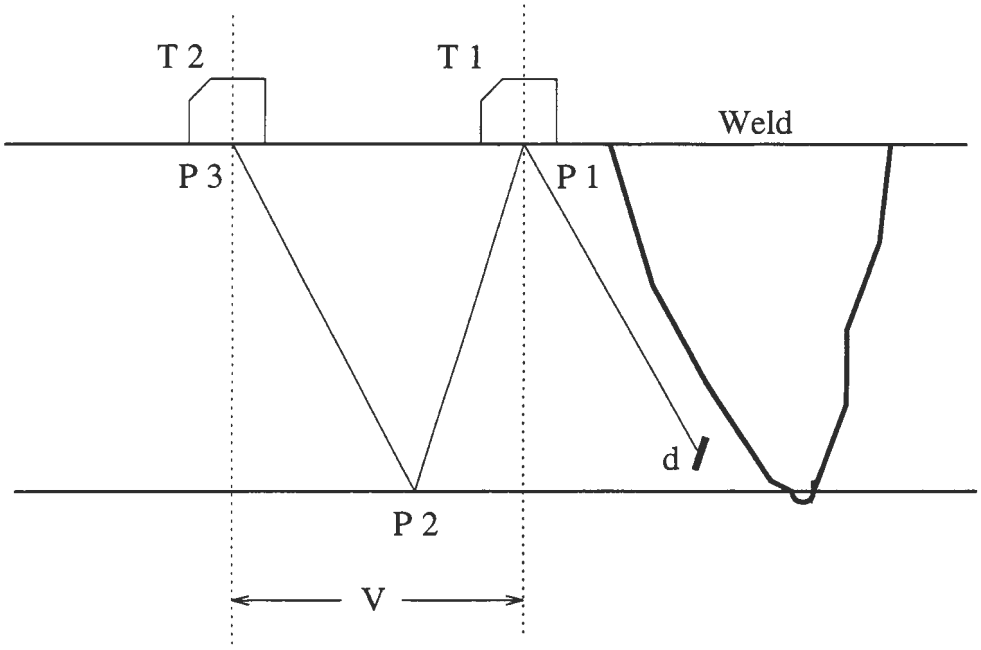

Figure 4.4: Periodic imaging of the same defect

that the metal-path traveled from all points on the face of the transducer is not the same. Thus the emerging beam is more in the shape of an ellipsoid, a phenomenon not encountered in normal SAFT.

The angle-beam SAFT procedure has to account for all these issues and complications. The corresponding angle-beam SAFT algorithm developed, is discussed in the following section.

Algorithm for Angle-Beam SAFT

The following algorithm outlines the major steps for performing angle-beam SAFT for a single depth position. It can be iterated over multiple depth positions to

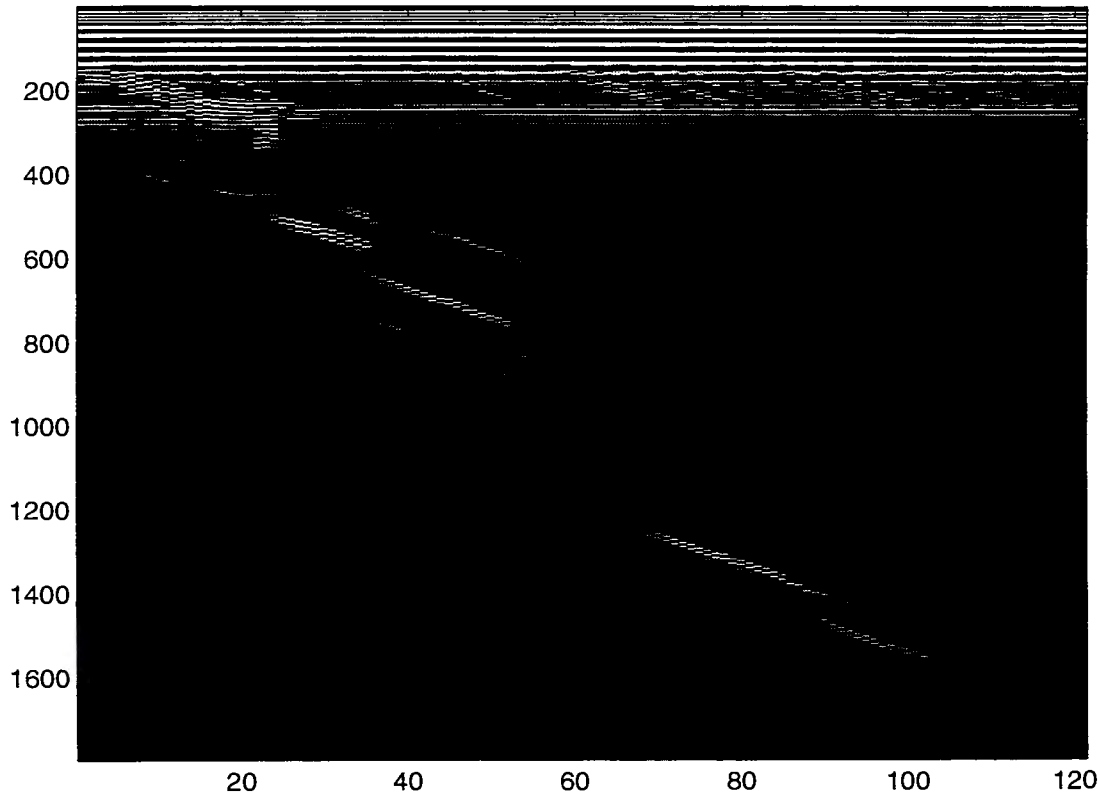

Figure 4.5: B-scan with periodic imaging of a crack

get the SAFT processing on multiple positions.

1. Input SAFT processing parameters: depth d, aperture α, thickness T, velocity of sound in specimen ϑ, angle of incidence θ, data sampling frequency S, total number of A-scans $numA$, and number of data points $numD$ in each A-scan. The parameters can be better recognized in Figure 4.6.

2. Read the set of A-scans constituting the B-scans $b{-}scans$ and the corresponding transducer positions pos. Initialize the result matrix $saft$ to 0.

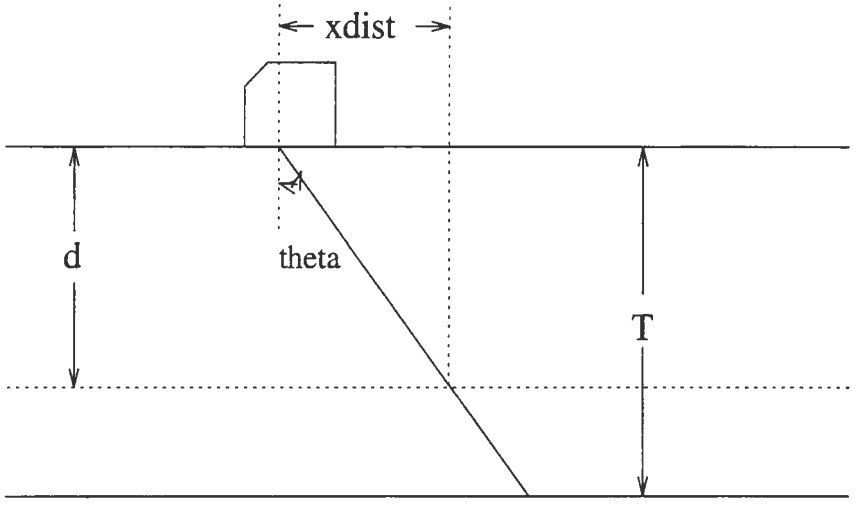

Figure 4.6: Test specimen geometry for the angle beam SAFT algorithm

3. Compute the lateral distance $xdist$ and metal path mp to the depth.

$$xdist = d \tan \theta \tag{4.4}$$

$$mp = 2\sqrt{d^2 + xdist^2} \tag{4.5}$$

The factor of 2 is included to take care of both the forward and backward path of the beam.

4. For $i = 1$: $numA$

   For $j = -a : a$

   Calculate the metal path $mpj(j)$ to the point P on the path of center of aperture (i) from the neighboring point $(i + j)$ as shown in Figure 4.7.

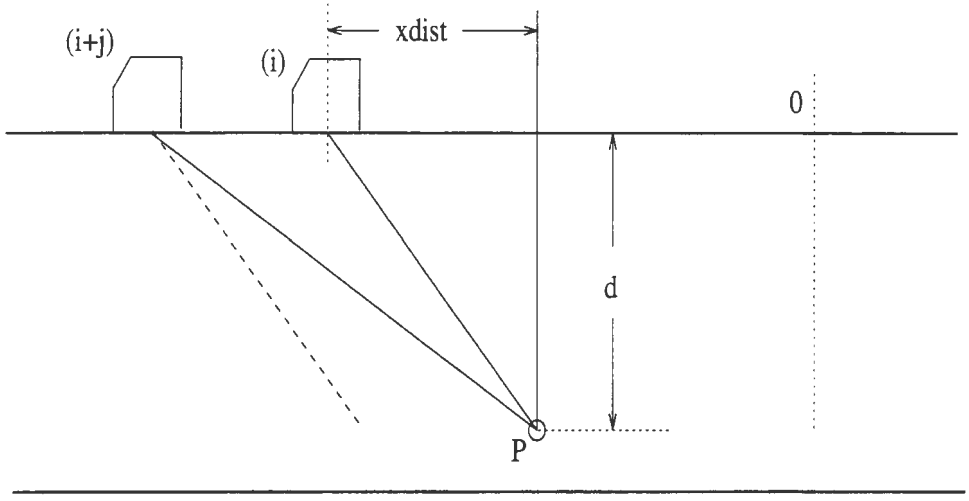

Figure 4.7: Metal path calculation geometry

$$mpj(j) = 2\sqrt{(pos(i+j) - pos(i) + xdist)^2 + d^2} \tag{4.6}$$

Calculate the time shift $ts(j)$ to be incorporated in the A-scan at point $(i+j)$

$$ts(j) = \frac{mpj(j) - mp}{\vartheta} * S \tag{4.7}$$

Shift the j^{th} scan and add to the result.

For $k = 1 : numD$

$$Saft(i,k) = Saft(i,k) + bscan(i+j, k+ts(j)) \tag{4.8}$$

end

end

end

5. Average the result over the aperture

$$Saft(i,k) = \frac{Saft(i,k)}{(2*a+1)} \tag{4.9}$$

This algorithm was implemented on a number of experimental B-scan images, and the results are presented in the following chapter.

Mapping between Image Domain and Physical Domain

The final goal of any image processing technique is to represent the result in a manner so that it is easy to interpret. It requires a fair amount of skill and practice to be able to map a point from an A-scan, to its corresponding location in the geometry of the specimen being inspected. Hence, mapping techniques, which will translate a point in an A-scan at a particular transducer position, to its corresponding position in the specimen, will greatly enhance visual interpretation. Preliminary mapping techniques to translate a point in an A-scan to its location in the geometry was done. The reverse mapping from the test geometry to the location in the A-scan was also developed. Both these techniques are described in the following sub-sections.

Mapping from image domain to physical domain

Mapping from the image domain to the physical domain implies that given the axial (a), and the circumferential (c) position of the transducer, along with a specific time of flight (tof), it is required to calculate the corresponding point (x, y, z), in the geometry of the test specimen. If v is the velocity of sound in the medium, then the metal path mp can be calculated as

$$mp = v * tof/2 \tag{4.10}$$

This can better understood by referring to Figure 4.8 The axial, x, circumferential,

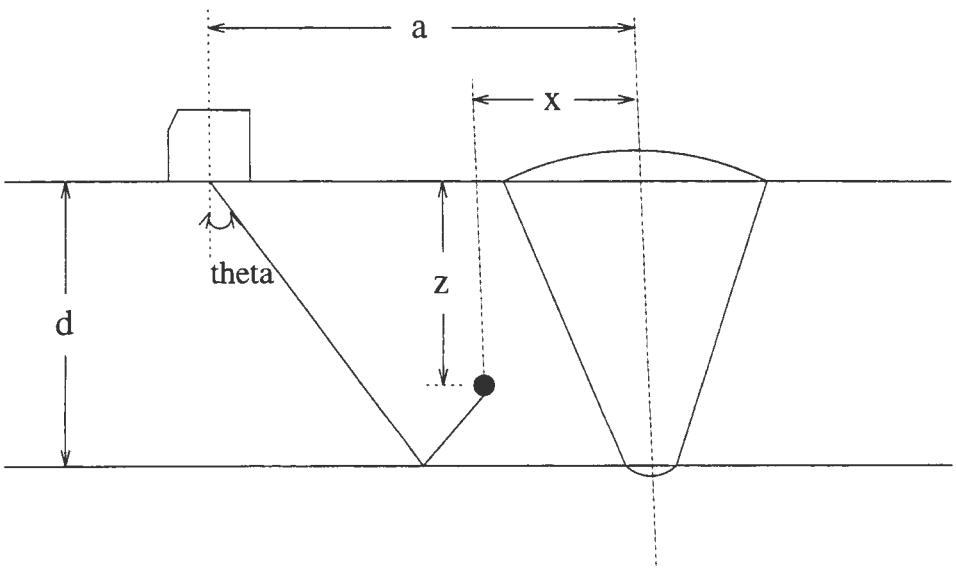

Figure 4.8: Mapping from image domain to physical domain

y, and depth, z, locatic·· of the point in the geometry can be calculated as

$$x = a - mp * sin\theta \tag{4.11}$$

$$y = c \tag{4.12}$$

$$z = (mp * cos\theta) modulo(d) \tag{4.13}$$

Here θ is the angle of incidence of the beam into the specimen, d is the thickness of the test specimen, and

Mapping from physical domain to the image domain

Mapping from the physical to the image domain implies that, given the axial (x), circumferential (y), and depth (z) location of a point in the specimen geometry, it is required to calculate the corresponding positions of the transducer (a, c), along with the time of flight tof, of the point in the A-scan record. In this case, as shown in the Figure 4.9, for each point in the geometry, there are two primary positions ($T1$ and $T2$) that need to be considered. One of them ($T1$) falls in the first half-V $(a1, c1, tof1)$, and the next ($T2$) in the second half-V $(a2, c2, tof2)$. In the first half-V, the location of the transducer and the corresponding time of flight is given by the following equations.

$$a1 = x + z * tan\theta \tag{4.14}$$

$$c1 = y \tag{4.15}$$

$$tof1 = 2 * z/(cos\theta * v) \tag{4.16}$$

In the second half-V, the equations for the calculations are as follows.

$$a2 = x + (d - z)/tan(\pi/2 - \theta) + d * tan\theta \tag{4.17}$$

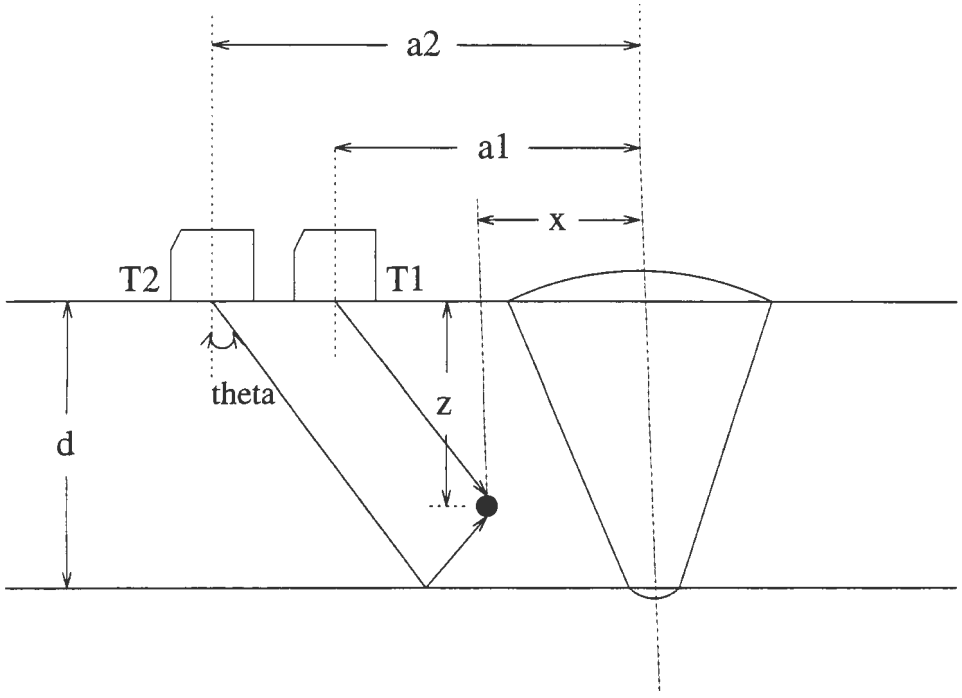

Figure 4.9: Mapping from physical domain to image domain

$$c2 = y \tag{4.18}$$

$$tof2 = 2 * (a2 - x)/(sin\theta * v) \tag{4.19}$$

Thus, using these equations, it is easy to map from one domain to another, thus enhancing visualization, and understanding. Following this, the next development is to use these functions to map the entire image information into an appropriate 3-dimensional representation of the geometry being imaged, along with the flaw representation.

CHAPTER 5. RESULTS AND DISCUSSIONS

The algorithm for performing angle-beam SAFT on B-scan images and B'-scan image was discussed in the previous chapter. In this chapter we present the results of implementing this algorithm on B-scan, B'-scans at single depths and multiple depths. This will be followed by the discussion of the results and finally the future work that can be carried out in this field.

Experimental Setup

The data for the SAFT system was obtained through the Electric Power Research Institute. In this section, a brief summary of the entire data collection scheme is given. In a typical setup, the UT process starts with an operator entering the reactor with his radiation-proof gear and the testing tools. Since most of the defects occur close to the weld, he uses normal incidence and angle beam incidence methods to check for reflections in the received echoes in those regions. On observing the reflection from a possible flaw, he moves the transducer in the neighboring regions to test if the reflection is from a defect or a counter-bore or the root of the weld.

All the above features produce distinct signatures in their corresponding reflections. For example, the reflections from a root weld are usually of a longer duration, whereas the reflection from the counterbore and the defect are much sharper. Again,

to distinguish between a counterbore and a crack, the operator moves the probe parallel to the counterbore. Since counterbore occurs throughout the pipe, reflections from counterbore will be present for all transducer positions along the circumference, whereas a crack can be characterized as a sharp reflection in a restricted neighborhood.

Following the detection of the flaw, the location and sizing of the flaw are done using the velocity of the wave, the thickness of the sample and the time of flight corresponding to the reflection.

In case of the data used for our experiments, standard 43^0 refracted beam was employed, with the same plastic wedges. All the pipes were stainless steel with a thickness of 0.69" and 12" outer diameters. The pipes were scanned using transducer probes centered at 1, 2.25, and 5 MHz. The analog received data was digitized using 8-bit analog-to-digital convertor. The reflected data was collected for $71.92\mu s$ for each of the transducer positions. This analog data was digitized at 25 Mega-samples/second to give A-scans of length 1798 samples each. A typical scan area was 3" X 10" with resolution of 0.025" (which is less than a quarter of a wavelength with velocity $\vartheta = 0.11$ inches/μs and frequency $f = 2.25MHz$) and 0.1" along the axis and circumference of the pipe, respectively. This led to individual data files which contains

$$\frac{3}{0.025} X \frac{10}{0.1} X 1798$$

samples

Thus each of the files was close to 22 MBytes in size.

Results

This section is divided into three parts, to present results of:

1. focusing at single depth for B-scan images
2. focusing at single depth for B'-scan images
3. focusing at multiple depths for B'-scan images

In all the sections, the test specimen is a stainless steel welded pipe of outer diameter 12" and thickness 0.69". The ultrasonic data was collected by a scanning a 3"(axial) by 10"(circumferential) region around the weld using angle-beam, pulse-echo technique. The center, frequency of the ultrasonic data was 2.25 MHz and the angle of inspection was 43^0. A plastic wedge was used to achieve this angle. The scanning was done in a raster format along the axial direction. The axial resolution is 0.025" and circumferential resolution is 0.1". The reflected analog data was collected for 71.92 μs for each of the transducer positions. This was then 8-bit sampled to give digital data of length 1798 for each of the A-scans. A wedge delay corresponding to 6.4 μs (or 16 samples) has to be compensated for, in each of the A-scans.

The pipe has a crack very close to the root of the weld. The circumferential span of the crack is 1.618" and depth is 0.33". The geometry of the pipe and the crack being imaged is illustrated in Figure 5.1

B-scan

As has been explained in an earlier section, B-scan is a collection of A-scans. In this case, the B-scan is in the axial direction, i.e. it has the higher resolution. A typical B-scan imaging is illustrated in Figure 5.2.

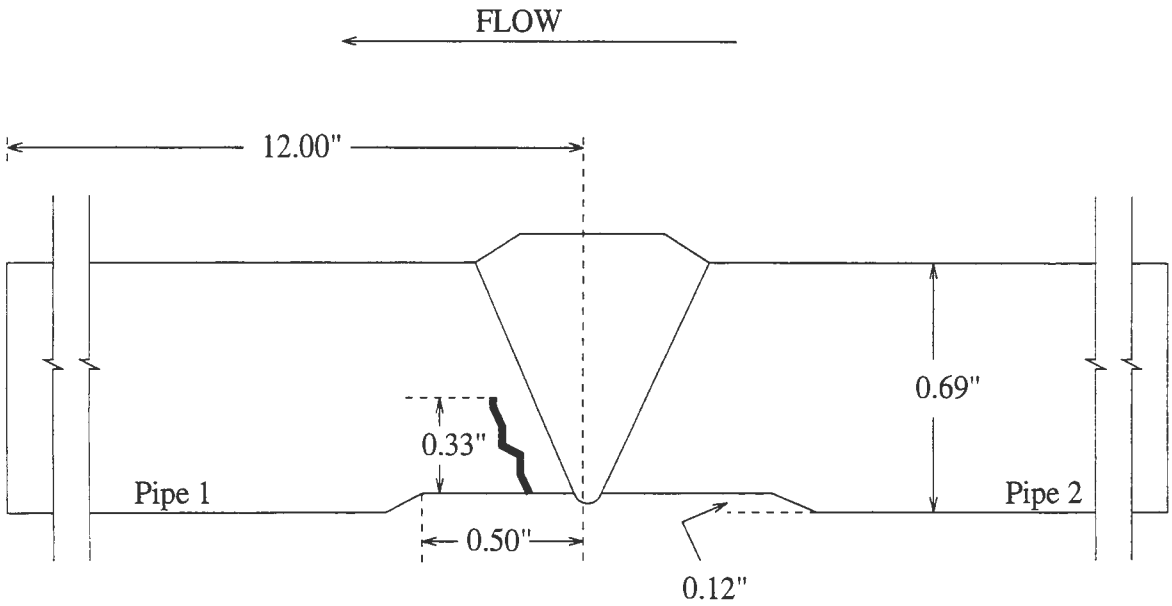

Figure 5.1: Experimental pipe geometry

The B-scan of the test specimen along a particular circumferential position is shown in Figure 5.3. As can be seen, there is a high saturation region in the initial part. This corresponds to the "big bang" or the reflection from the front wall-wedge interface.

As the transducer, moves away from the weld, during the B-scan imaging, the defect and the weld are seen at later positions in time or the time of flight (TOF).

Note that, because of the periodicity in angle-beam imaging the same reflections are periodically repeated at a large TOF for the transducer position further away from this weld.

The transducer raster scans in the same directions as in B-scan imaging. As a

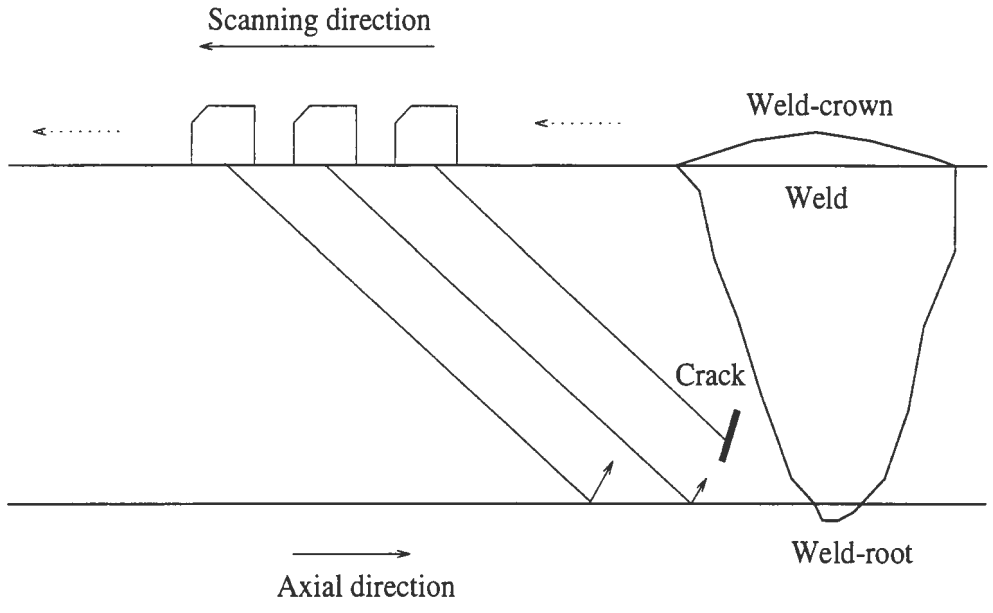

Figure 5.2: B-scan imaging

result, the higher resolution of 0.025" is in this direction. Consequently, SAFT can be applied over a larger aperture, since because of the physical proximity between the transducer locations for the B-scan, the same reflectors can be seen over a larger windows of A-scans. Figure 5.4 shows the result of SAFT performed on the B-scan in Figure 5.3. The aperture chosen was 10 and the depth of the SAFT corresponds to the third leg.

The third leg was chosen, because of two reasons:

1. Due to the high gain of the receiving amplifier in the scanning system, to be able to detect the smallest flaws, the data is highly saturated in the first leg of the beam and hence this leg could not be used.

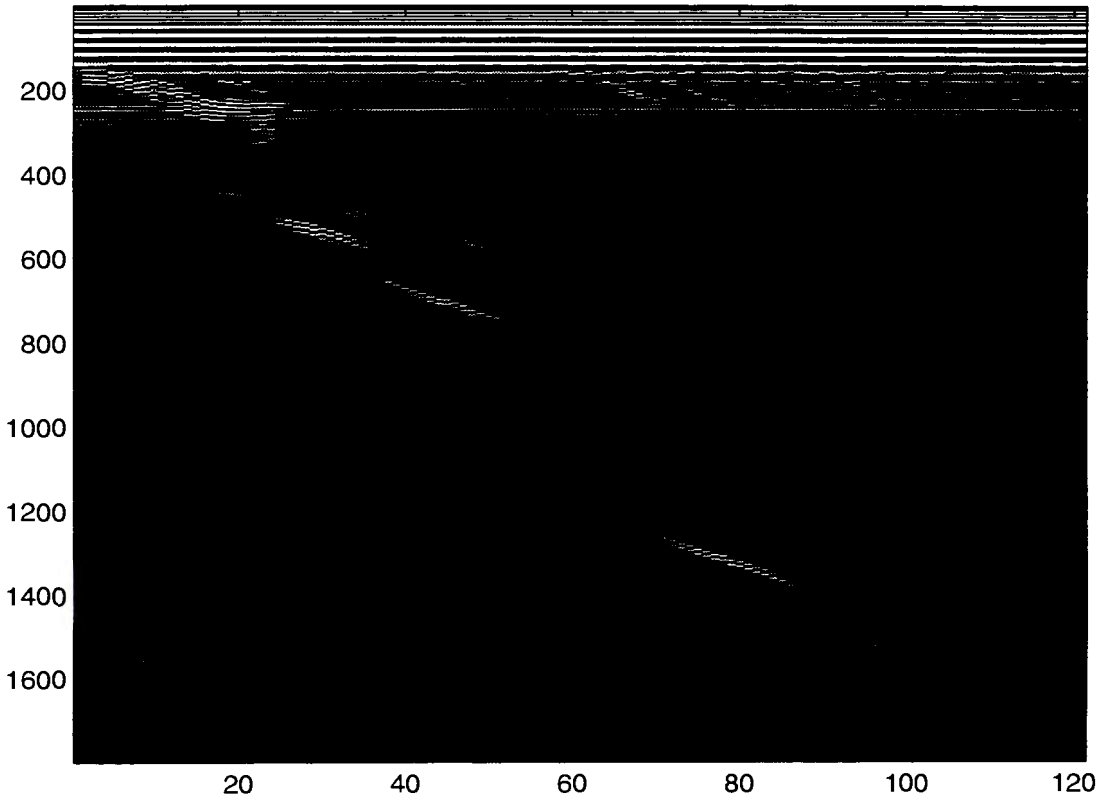

Figure 5.3: A B-scan image in which the defect can be seen clearly

2. There is a larger beam spread in the third leg and hence contributions from the reflectors occur over a larger area, thus improving the ability of the SAFT algorithms.

Another B-scan image in which the defect or the weld are not seen clearly is illustrated in the Figure 5.5. The result of performing SAFT with an aperture size of 10 is illustrated in Figure 5.6.

As can be seen, there is clearly an improvement in the resultant image after performing the SAFT, as the flaw and the weld-reflections can be made out more

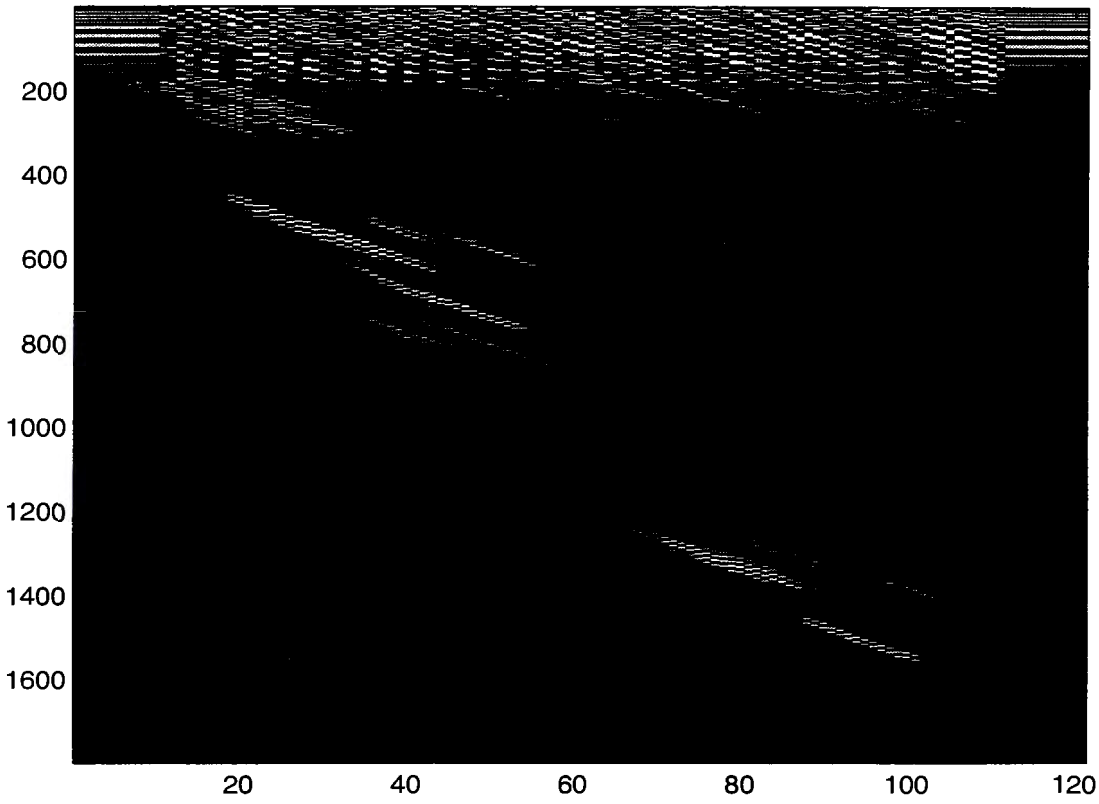

Figure 5.4: After SAFT implementation on the B-scan

clearly.

B'-scan

The B-scan imaging is a collection of consecutive A-scans along the axial direction. The B'-scan, on the other hand, is a collection of consecutive A-scans along the circumferential direction. This is illustrated the Figure 5.7. Since the transducer moves parallel to the weld and the crack in the corresponding B'-scan image, they are "seen" at the same time of flight (TOF).

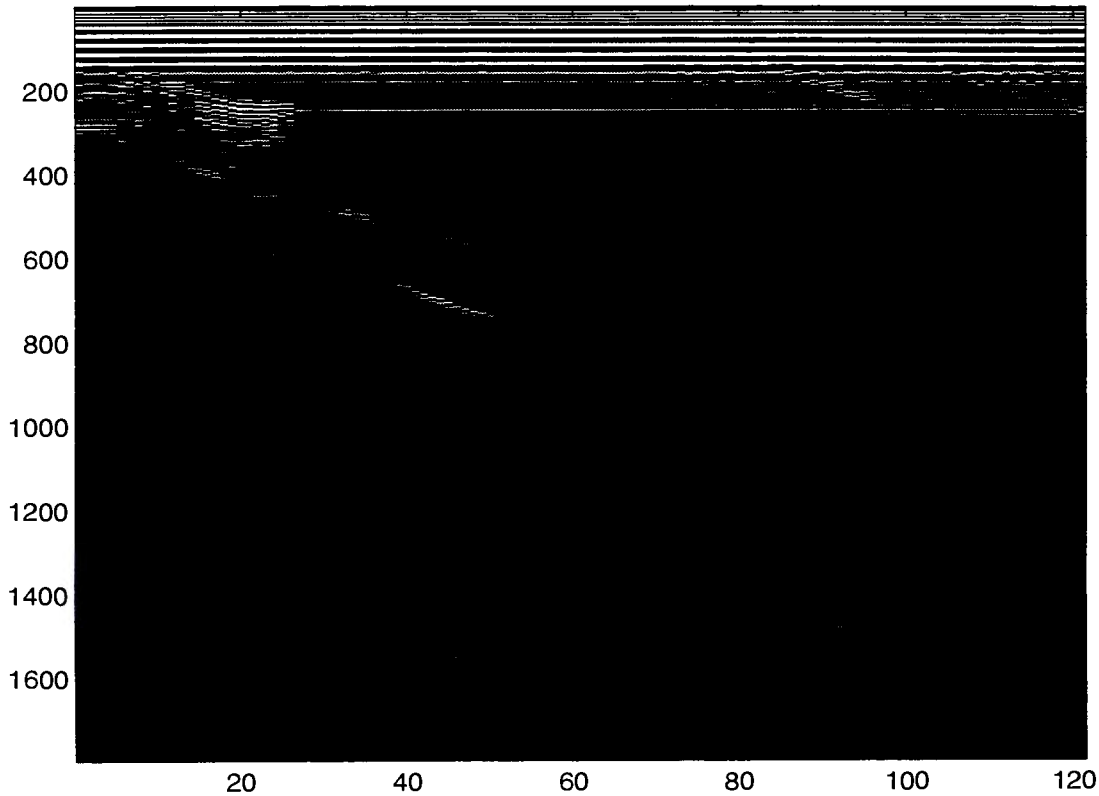

Figure 5.5: A B-scan image in which the defect cannot be seen clearly

Note that the periodicity of the reflection is not observed in a B'-scan imaging, since the transducer is being moved parallel to the weld.

Since the transducer scans along the lower resolution axis, SAFT is performed over a small aperture size as compared to the B-scan case. Figure 5.8 shows a B'-scan from the pipe, along a certain axial position.

Due to the reasons explained in the B-scan imaging the SAFT algorithm has been implemented for the third leg of the beam. The B'-scan has been chosen such that the defect lies in the third leg. The aperture size chosen is 3 because of the

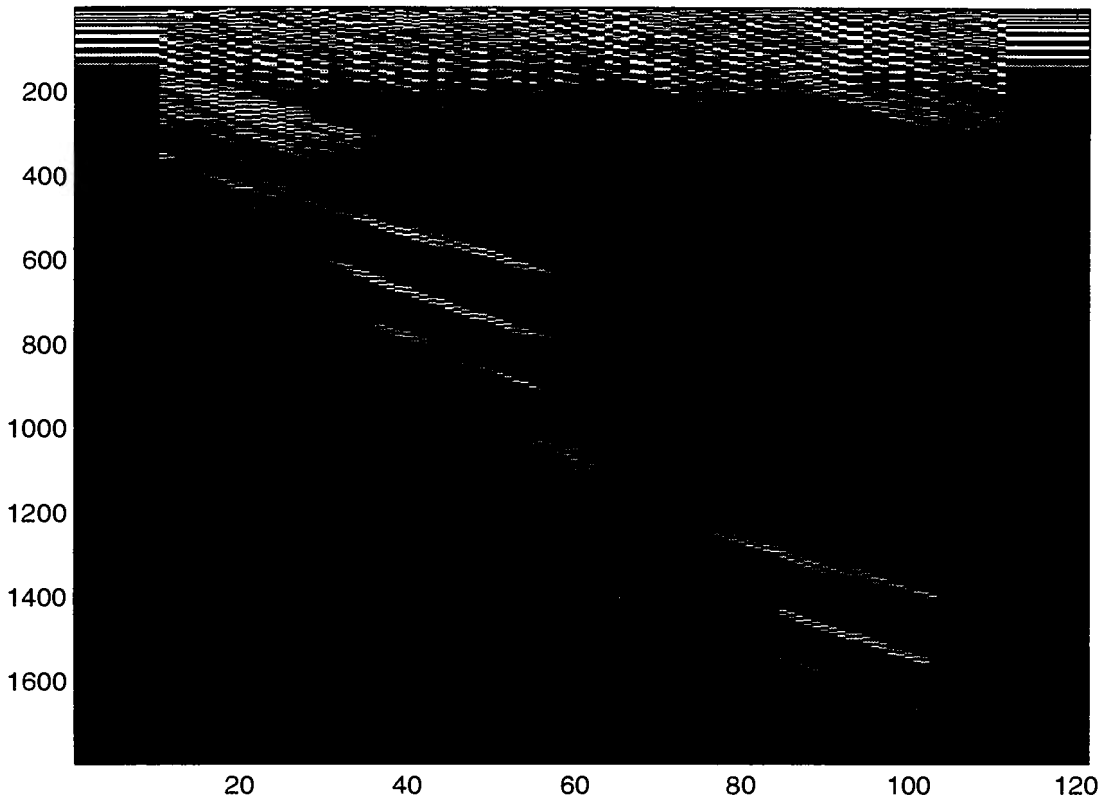

Figure 5.6: After SAFT implementation on the B-scan

lower resolution along the circumferential direction. Figure 5.9 shows the result of the SAFT algorithm.

Figure 5.10 shows a comparatively degraded B'-scan image. Figure 5.11 illustrates SAFT with aperture size 3

As can be seen, there is an improvement in the detection ability after performing the B'-scan SAFT.

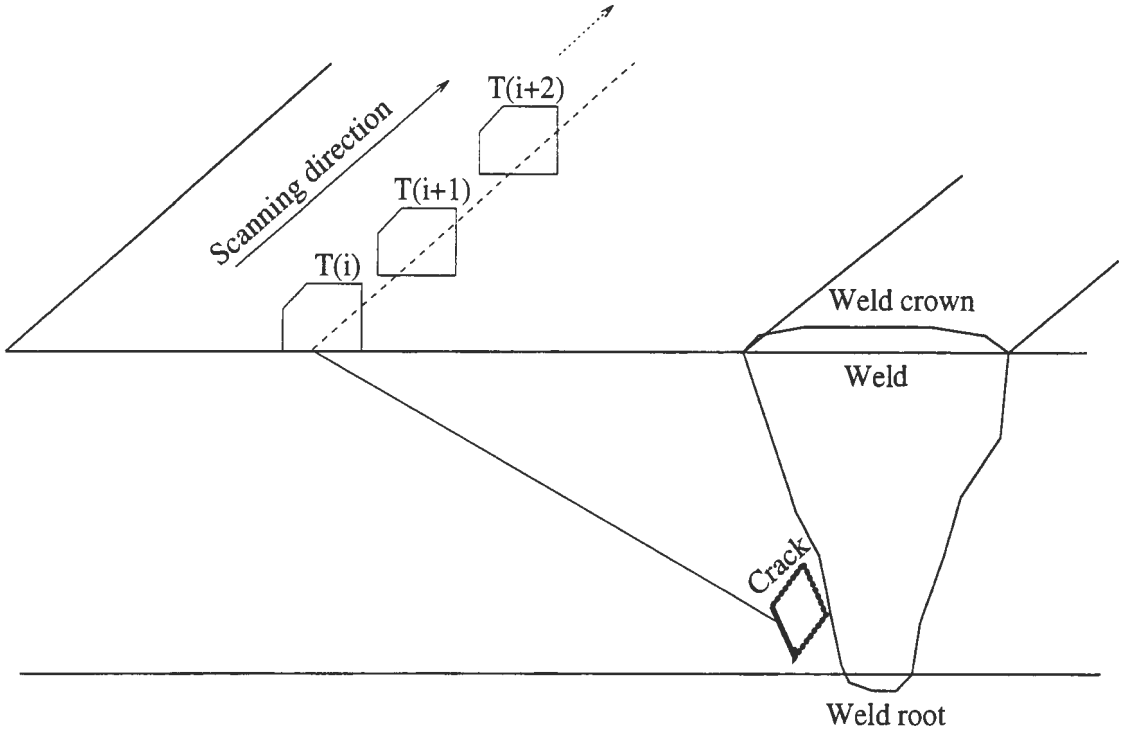

Figure 5.7: B'-scan imaging technique

Multi depth B'-scan

During the multidepth implementation of the SAFT algorithm, the B'-scan image of Figure 5.12 was selected. The SAFT was then performed at 6 uniformly spaced depths in the third leg. The resultant images were then combined to give Figure 5.13. As can be seen, in Figure5.13 the flaw profile comes up very clearly, due to focusing at more than one depths. Thus, performing multidepth SAFT is definitely a better technique than single depth focusing.

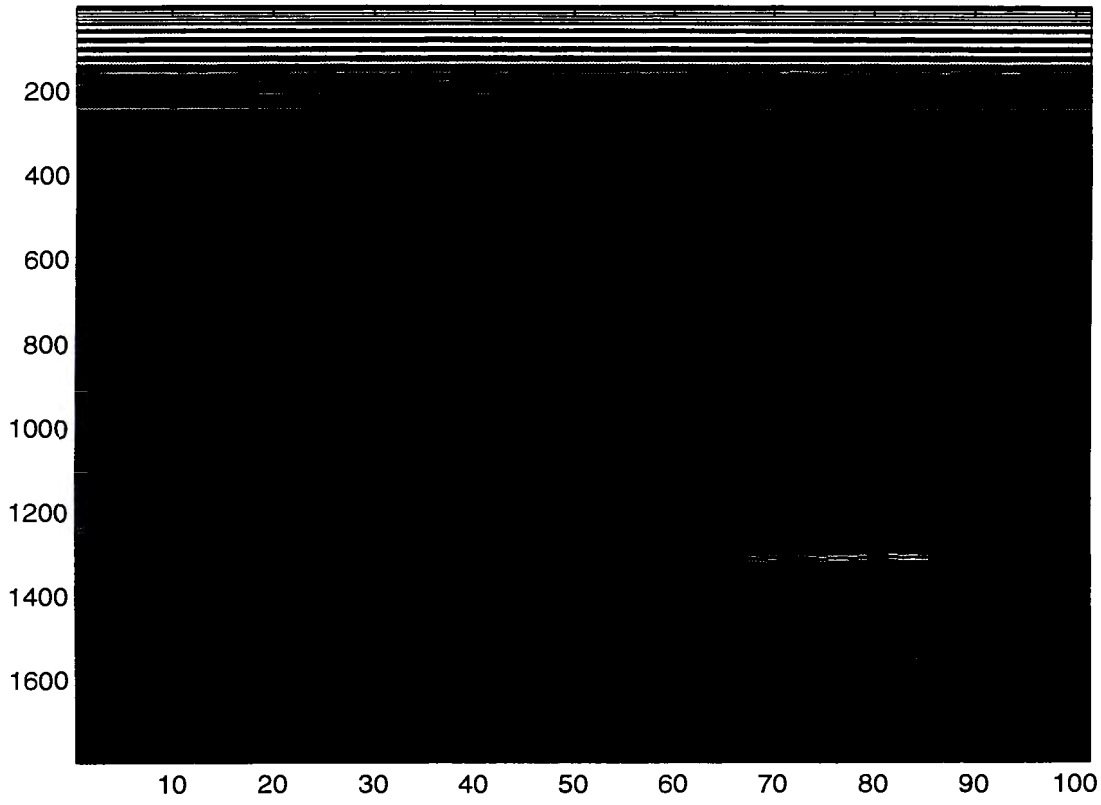

Figure 5.8: A B'-scan image in which the defect can be seen clearly

Discussion

As can be seen from the results in the previous sections, SAFT is indeed a valuable tool, to enhance ultrasonic testing techniques, to take care of the complex scattering phenomenon.

The depth of SAFT requires to be known apriori. Also the aperture size needs to be directly related to the scanning resolution in the particular direction. If the aperture size chosen is too large, besides the additional computational complexity, there might be severe degradation of the resultant image. This is because the im-

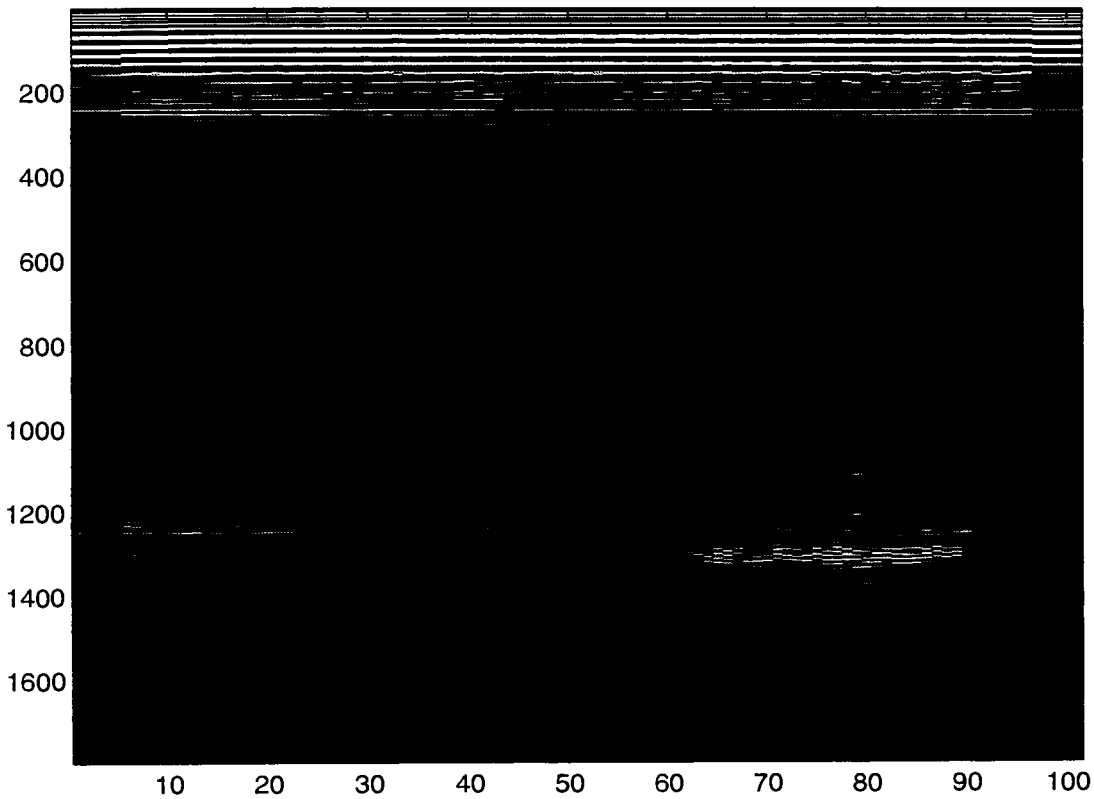

Figure 5.9: After SAFT implementation on the B'-scan

plementation would average over A-scans in which there is no contribution from the defect. This definitely needs to be avoided.

B'-scan imaging is better than B-scan imaging in this particular research. This is because, the orientation of the cracks makes the B'-scan more perceptible, visually, as it is easier to distinguish the weld and crack regions more clearly in the B'-scan image. However, in this research, because of the higher resolution in the B-scan direction, there is a larger area (or transducer positions) to which a reflector contributes.

Multidepth-focusing is a good option in this case, since the crack can be at any

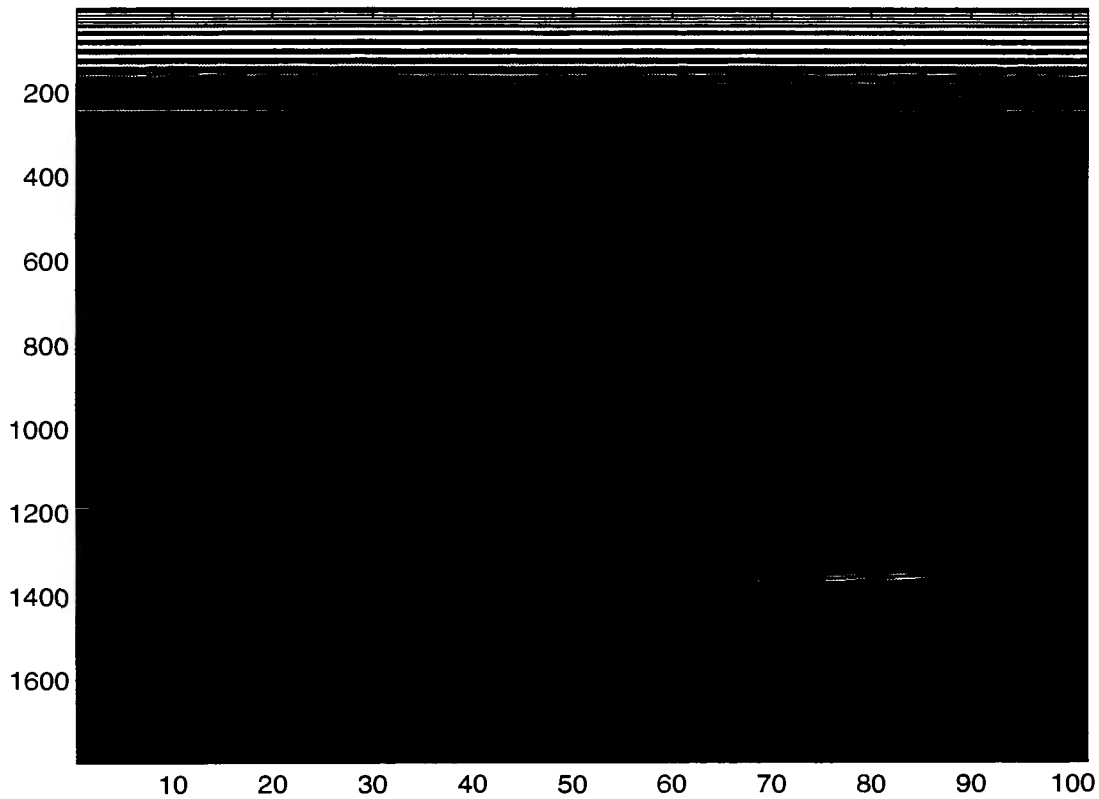

Figure 5.10: A B'-scan image in which the defect cannot be seen clearly

depth in the specimen. By attempting to focus at multiple depths, the amount of apriori information required is reduced. Secondly, flaw profiles not envisaged, might be seen in the same B'-scan after processing it via the SAFT algorithm.

The work reported in this thesis on the application of SAFT to angle-beam pulse-echo ultrasonic testing technique clearly shows that this methodology is quite powerful at achieving an improved resolution.

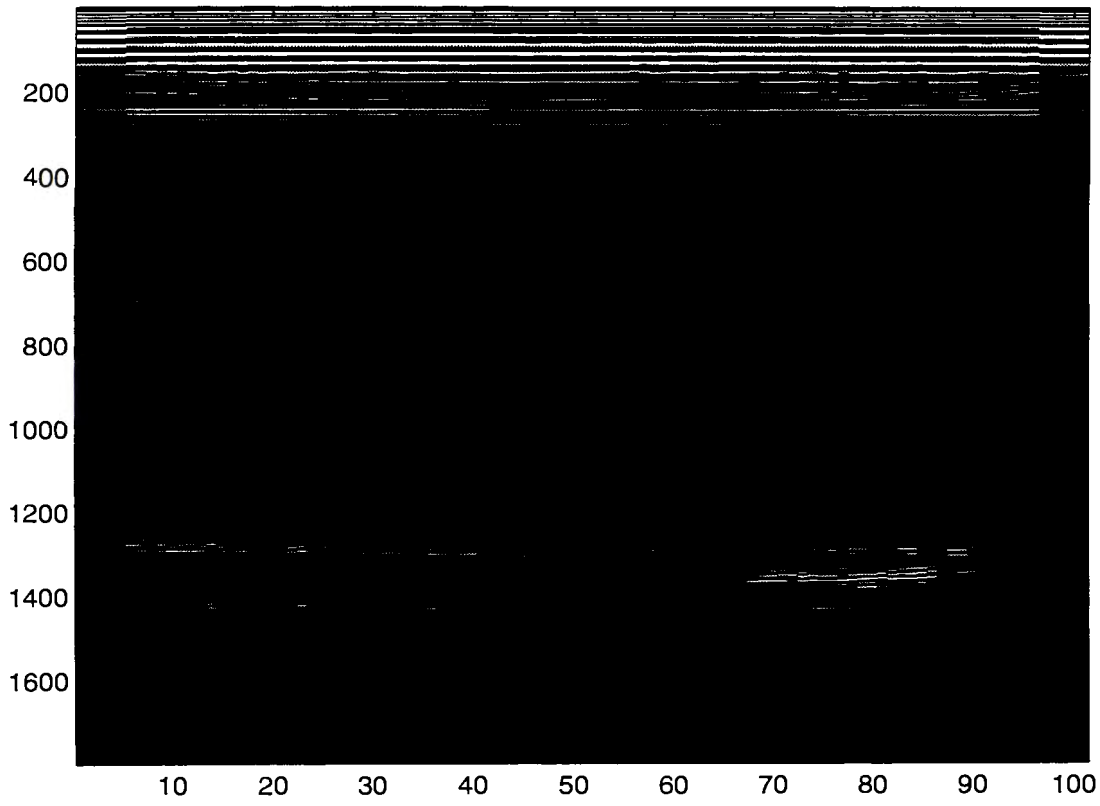

Figure 5.11: After SAFT implementation on the B'-scan

Conclusion

Angle-beam pulse echo technique is the dominant mode of data collection in the nuclear industry. The data obtained, however, is very noisy, and signal processing techniques are needed to enhance the signal-to-noise ratio of this data, to improve operator interpretation. Focus has been placed on SAFT as a technique to perform this noise reduction and resolution improvement. SAFT is a valuable tool, for ultrasonic NDE because of the complex scattering phenomenon in the weld material. Most of the research done earlier, has been in the field of normal SAFT. However,

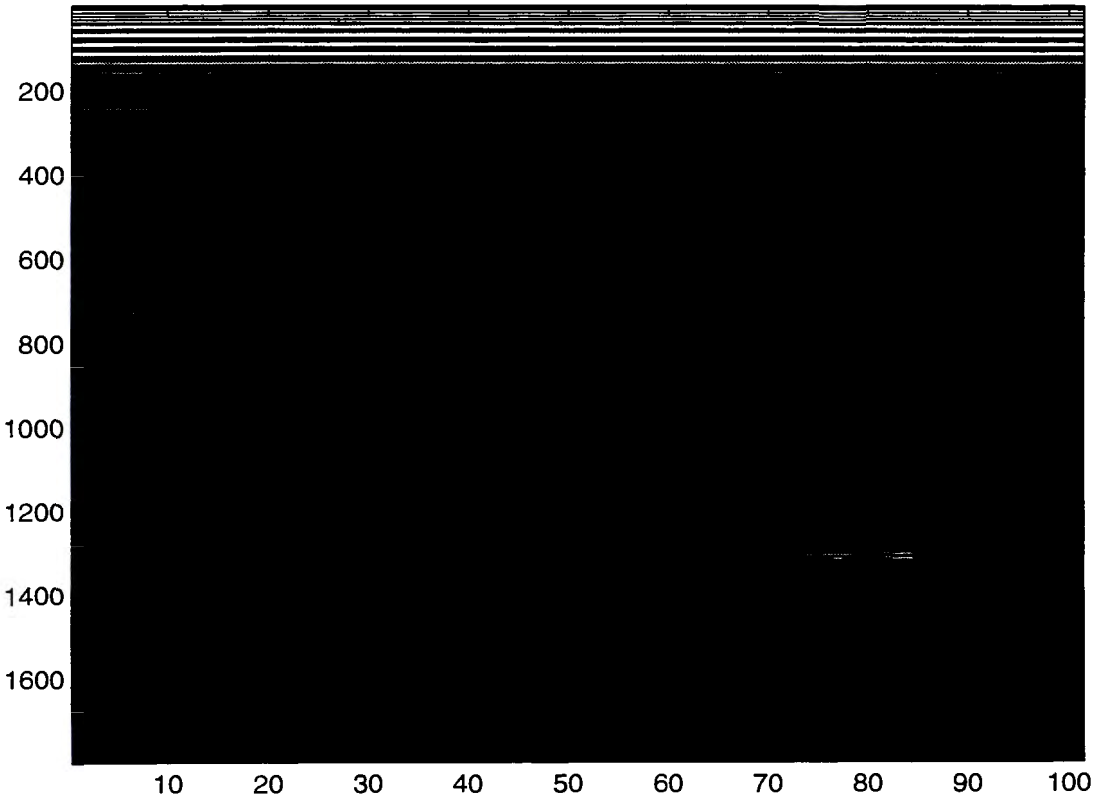

Figure 5.12: A B'-scan image in which the defect cannot be seen clearly

the algorithm for normal SAFT has to be enhanced, to incorporate issues unique to the angle-beam mode of data collection. These include multiple sound paths of the ultrasonic beam, and spatial periodicity of the defects. The angle-beam SAFT algorithm was developed in this research.

Flaw location is very important in the nondestructive evaluation of a specimen. However, it is also very difficult. In this research, algorithms have been developed to aid in manual and computer flaw location.

From the results of performing SAFT on various B-scan and B'-scan images, it

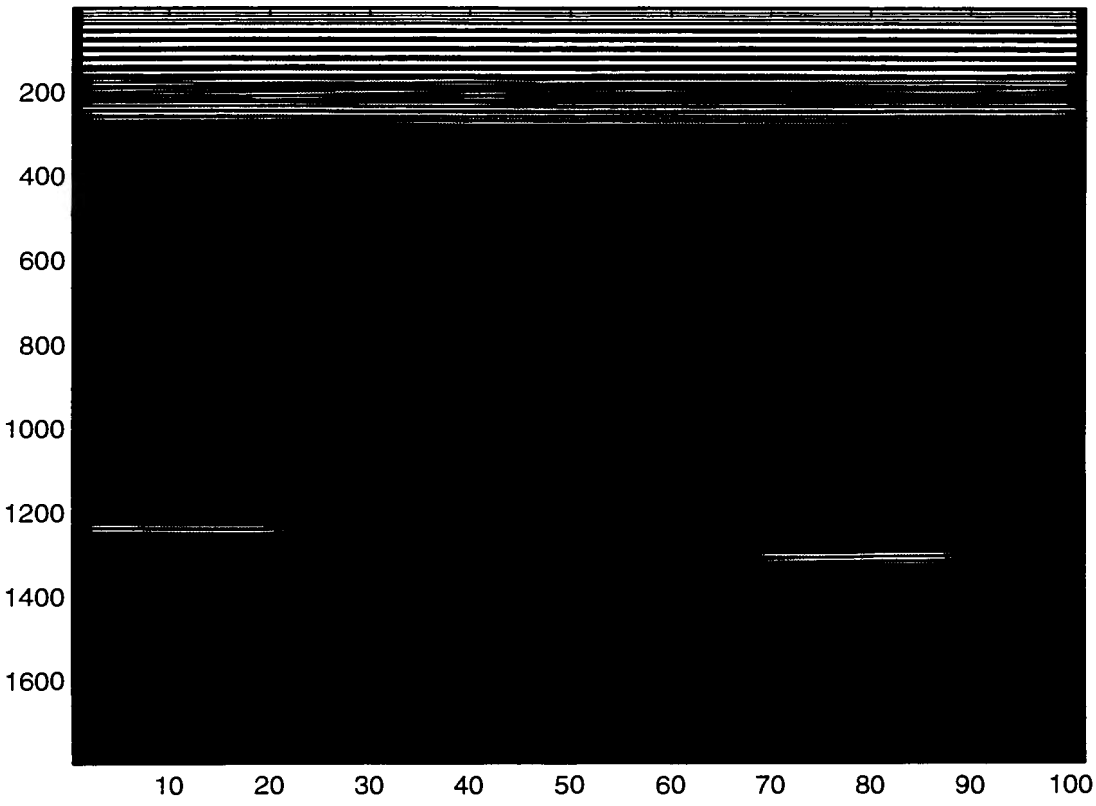

Figure 5.13: After implementing SAFT at 6 uniformly spaced depths in the third leg of the B'-scan

can be concluded that SAFT is indeed a valuable tool for improvement of ultrasonic images of nuclear tubings.

Future Work

Further development and refinement of the SAFT process is desirable, in order to consider all possible factors. Proposals for additional studies may include the following avenues:

1. The algorithm should be developed independent of the apriori information required for the SAFT depth calculation. This could be done using a neural network approach, which produces the data set to detect possible defects. The neural network could inform the SAFT algorithm about the approximate location of the defect.

2. The optimum aperture size for a given scanning geometry could be calculated automatically. This can be done using the basic laws of physics to calculate the beam spread in the test specimen using the sound wavelength, the ultrasonic impedance of the test material and the scanning resolution in the particular direction.

3. As a final suggestion, to optimize the inherent capabilities of SAFT, the possible expansion to real-time should be looked into, as a way to speed up the computational time. Due to the fact that the SAFT-algorithm executes its computation A-scan by A-scan, and the process is repeated for each of the A-scan, all individual operations can be parallelized via the use of an array processor. This may reduce the CPU-time by a large factor, which may be a critical requirement in an extensive testing environment.

BIBLIOGRAPHY

[1] Singh, A. (1980). *Crack Depth Determination by Ultrasonic Frequency Analysis Aided by Dynamic Photoelasticity.* Ames, IA: Iowa State University.

[2] Gordon P. H. (1978). *Introduction to Nondestructive Testing.* Milwaukee, WI: American Society for Quality Control.

[3] Halmshaw, R. (1987). *Non-destructive Testing.* London, UK: Edward Arnold Publications.

[4] Fordham, P. (1968). *Non-destructive Testing Techniques.* London, UK: London Business Publications Limited.

[5] Ghorayeb, S. (1992). *Study of Beamforming Techniques for Ultrasound Imaging in Nondestructive Testing.* Ames, IA: Iowa State University.

[6] Kessler, L. W. (1989). Acoustic Microscopy *Metals Handbook 17.* Materials Park: ASM International.

[7] Havlice, J. F. and Taenzer, J. C. (1979). Medical Ultrasound Imaging: An Overview of Principles and Instrumentation. *Proc. IEEE 67*: 620-641.

[8] Haumschild, D. J. and Carlson, D. L. (1983). An Ultrasonic Bragg Scattering Technique for the Quantitative Characterization of Marbling in Beef. *Ultrasonics 21*: 226-233.

[9] Macovski, A. (1983). *Medical Imaging Systems.* Englewood Cliffs, NJ: Prentice-Hall.

[10] Woodcock, J. P. (1979). *Ultrasonics: Medical Physics Handbook 1.* Bristol, UK: Adam Hilger.

[11] Seydel, J. (1982). *Research Techniques in Nondestructive Testing.* London, UK: Academic Press.

[12] Langenberg, K. J., Berger, M., Kreutter, T., Mayer, K. and Schmitz, V. (1986). Synthetic Aperture Focusin Technique Signal Processing. *NDT International 19*: 177-188.

[13] Heyman, E. and Felsen, L. B. (1985). A Wavefront Interpretation of the Singularity Expansion Method. *IEEE tranaction on Antenna Propagation 33*: 706-720.

[14] Langenberg, K. J., Aulenbacher, U., Bollig, G., Fellinger, P., Weinfurter, J. and Zanger, P. (1986). Pulsed Wave Scattering: Wavefronts and Resonances, identification and Imaging. *IEEE tranaction on Antenna Propagation 33*: 312-321.

[15] Furniturewala, I., Udpa, L. and Udpa, S. (1995). Angle Beam Synthetic Aperture Focusing in Ultrasonics. *Proceedings of the 4th Annual Midwest Electro-Technology Conference*: 100-103.

[16] Doctor, S. R., Hall, T. E. and Reid, L. D. (1986). SAFT - The Evolution of a Signal Processing Technology for Ultrasonic Testing. *NDT International 19*: 163-167.